JACS
JOURNAL OF THE AMERICAN CHEMICAL SOCIETY
Article
pubs.acs.org/JACS

# Tuning of Charge Transfer Assisted Phase Transition and Slow Magnetic Relaxation Functionalities in $\{Fe_{9-x}Co_x[W(CN)_8]_6\}$ ($x$ = 0−9) Molecular Solid Solution

Szymon Chorazy,[†,‡] Jan J. Stanek,[§] Wojciech Nogaś,[†] Anna M. Majcher,[§] Michał Rams,[§] Marcin Kozieł,[†] Ewa Juszyńska-Gałązka,[∥] Koji Nakabayashi,[‡] Shin-ichi Ohkoshi,[*,‡] Barbara Sieklucka,[†] and Robert Podgajny[*,†]

[†]Faculty of Chemistry, Jagiellonian University, Ingardena 3, 30-060 Kraków, Poland
[‡]Department of Chemistry, School of Science, The University of Tokyo, 7-3-1 Hongo, Bunkyo-ku, Tokyo 113-0033, Japan
[§]Institute of Physics, Jagiellonian University, Łojasiewicza 11, 30-348 Kraków, Poland
[∥]H. Niewodniczański Insitute of Nuclear Physics PAN, Radzikowskiego 152, 31-342 Kraków, Poland

Supporting Information

**ABSTRACT:** Precisely controlled stoichiometric mixtures of $Co^{2+}$ and $Fe^{2+}$ metal ions were combined with the $[W^V(CN)_8]^{3-}$ metalloligand in a methanolic solution to produce a series of trimetallic cyanido-bridged $\{Fe_{9-x}Co_x[W(CN)_8]_6(MeOH)_{24}\}\cdot 12MeOH$ ($x$ = 0, 1, ..., 8, 9; compounds **0**, **1**, ..., **8**, **9**) clusters. All the compounds, **0**−**9**, are isostructural, and consist of pentadecanuclear clusters of a six-capped body-centered cube topology, capped by methanol molecules which are coordinated to 3d metal centers. Thus, they can be considered as a unique type of a cluster-based molecular solid solution in which different Co/Fe metal ratios can be introduced while preserving the coordination skeleton and the overall molecular architecture. Depending on the Co/Fe ratio, **0**−**9** exhibit an unprecedented tuning of magnetic functionalities which relate to charge transfer assisted phase transition effects and slow magnetic relaxation effects. The iron rich **0**−**5** phases exhibit thermally induced reversible structural phase transitions in the 180−220 K range with the critical temperatures being linearly dependent on the value of $x$. The phase transition in **0** is accompanied by $^{HS}Fe^{II}$ $W^V \leftrightarrow {}^{HS}Fe^{III}$ $W^{IV}$ charge transfer (CT) and the additional minor contribution of a Fe-based spin crossover (SCO) effect. The Co-containing **1**−**5** phases reveal two simultaneous electron transfer processes which explore $^{HS}Fe^{II}$ $W^V \leftrightarrow {}^{HS}Fe^{III}$ $W^{IV}$ CT and the more complex $^{HS}Co^{II}$ $W^V \leftrightarrow {}^{LS}Co^{III}$ $W^{IV}$ charge transfer induced spin transition (CTIST). Detailed structural, spectroscopic, and magnetic studies help explain the specific role of both types of $CN^-$-bridged moieties: the Fe-NC-W linkages activate the molecular network toward a phase transition, while the subsequent Co−W CTIST enhances structural changes and enlarges thermal hysteresis of the magnetic susceptibility. On the second side of the **0**−**9** series, the vanishing phase transition in the cobalt rich **6**−**9** phases results in the high-spin ground state, and in the occurrence of a slow magnetic relaxation process at low temperatures. The energy barrier of the magnetic relaxation gradually increases with the increasing value of $x$, reaching up to $\Delta E/k_B$ = 22.3(3) K for compound **9**.

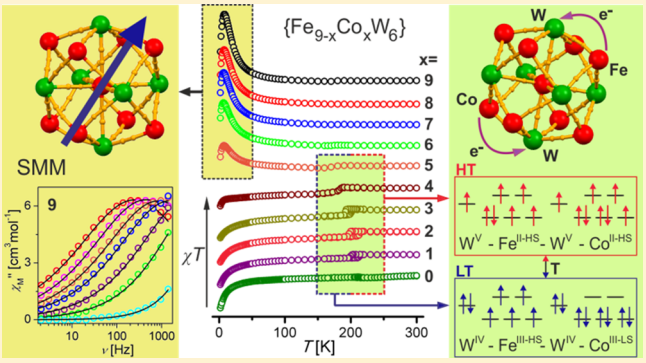


## INTRODUCTION

The demand of external control over a state of matter is unceasingly a driving force in the continuous research of new functional materials, especially those which combine a few different physical properties. Such multifunctionality can be achieved within the area of soft molecular materials which incorporate a variety of building blocks. The building blocks can include those which bear some intrinsic prerequisites for functionality, as well as those which have potential to assemble toward more extended functional synthons by exploiting the interplay between structural, chemical and physical properties. This approach enables the coexistence of different properties, including structural transition, porosity, electron transfer, magnetism, conductivity, chirality, luminescence and others, in one molecular network.[1−7] Moreover, it gives the opportunity to design new materials for reversible multichannel external stimulation, as observed in photomagnets or multiferroics,[8,9] as well as for specific tuning of the output light due to second order magneto-optical effects, as reported for optical and chiral molecule-based magnets.[10]

In this regard, the polynuclear cyanido-bridged systems provide the efficient and versatile molecular platforms of interest,

**Received:** November 14, 2015
**Published:** January 13, 2016



DOI: 10.1021/jacs.5b11924
J. Am. Chem. Soc. 2016, 138, 1635−1646

as they combine intermetallic local magnetic coupling or long-range magnetic ordering with externally ($T$, $hv$, $p$, guest) controlled reversible structural phase transitions, accompanied by charge/electron transfer induced spin transition (CTIST) or spin crossover (SCO) phenomena.[3,8] The SCO or CTIST effects in such systems offer the ability of thermally reversible switching between different spin states at high temperature, while at low temperature, the more prominent magnetization/demagnetization processes can be induced by the light irradiation due to light induced excited spin state trapping (LIESST) phenomenon.[8] To achieve this, a rational incorporation of redox or SCO active d-metal ions into the molecular coordination skeleton is necessary. Several combinations of such cyanido-bridged building blocks were established during the past decade, and they include prominent $Co^{II/III}$-$[Fe^{III/II}(CN)_6]^{3-/4-}$,[3a,b,11] $Co^{II/III}$-$[Fe^{III/II}(L)(CN)_3]^{-}$,[8d,12] $Co^{II/III}$-$[Os^{III/II}(CN)_6]^{3-/4-}$,[3d] $Co^{II/III}$-$[W^{V/IV}(CN)_8]^{3-/4-}$,[13] $Mn^{II/III}$-$[Fe^{III/II}(CN)_6]^{3-/4-}$,[3c] $Fe^{II}$-$[Fe^{III}(3L)(CN)_3]^{-}$ (3L = tridentate ligand),[8c,14] $Fe^{II}$-$[Nb^{IV}(CN)_8]^{4-}$,[8a,10c,15] as well as the very new and promising $Fe^{II/III}$-$[Os^{III/II}(CN)_6]^{3-/4-}$,[16] $Fe^{III/II}$-$[W^{V/IV}(CN)_8]^{3-/4-}$,[17] or $Ni^{III/II}$-$[Fe^{II/III}(CN)_6]^{4-/3-}$ pairs.[18]

Among these systems, a particular interest is paid to zero-dimensional molecules and one-dimensional chains which allow the combination of externally controllable phase transitions with the effect of slow relaxation of magnetization below blocking temperature owing to the strong uniaxial magnetic anisotropy.[19−23] These extraordinary molecular objects, referred to as single molecule magnets (SMM) and single chain magnets (SCM), exploit the magnetic anisotropy of d[20] and 4f/5f metal ions,[21] and 3d−4f combinations,[22] including cyanido-bridged assemblies.[23] When externally stimulated phase transitions are also embedded, it becomes possible to design switchable single molecule magnets and single chains magnets in which the slow magnetic relaxation can be reversibly induced or canceled, for instance, by light irradiation.[14] This route also offers an additional and independent way to control the magnetic state by switching in the 0 → 1 → 0 sequence. Thus, the performance of currently used standard molecular model device-systems which exploit electronic read-out and transverse field technique should be further developed, and is of a great importance in a face of future technological demand for data storage and processing.[24]

Over the last few decades, the diversity of low dimensional cyanido-bridged coordination structures has been found to range from simple low-nuclearity oligomers to cage or cluster forms,[11,12c,25,26] up to 42-nuclear giant molecules.[27] On the intricate way toward the nuclearity limits, several polyhedral structural motifs appeared in a systematic and repeating manner.[25] A pentadecanuclear six-capped body-centered cube topology (Figure 1) has attracted particular interest as it was widely adopted by bimetallic clusters of a general $\{M^{II}_9[M'^{V}(CN)_8]_6\}$, $\{M_9M'_6\}$ (M = Mn, Fe, Co, Ni; M′ = W, Mo, Re) composition,[17,28] and by trimetallic $\{M_{(1)}{}^{II}_xM_{(2)}{}^{II}_{9-x}[M'^{V}(CN)_8]_6\}$ or $\{M^{II}_9[M_{(1)}{}'^{V}(CN)_8]_y[M_{(2)}{}'^{V}(CN)_8]_{6-y}\}$ assemblies with two different M or M′ metal centers of similar ionic radii, e.g., $Co^{II}/Fe^{II}$ as M sites,[29] or $W^{V}/Re^{V}$ as M′ sites.[30] This family of molecules demonstrates magnetic coupling which leads to high-spin ground states, up to $^{39}/_2$ for $\{Mn^{II}_9W^{V}_6\}$.[28a] By using selected anisotropic 3d metal centers, the single molecule magnet (SMM) behaviors could also be detected, as exemplified by purely solvated $\{Co^{II}_9W^{V}_6\}$,[28b] and tmphen-capped $\{Ni^{II}_9W^{V}_6\}$ (tmphen = 3,4,7,8-tetramethyl-1,10-phenanthroline) clusters.[31]

Our recent studies, which were focused on $\{Co_9W_6\}$,[32] $\{Fe_6Co_3W_6\}$,[29] $\{Fe_9W_6\}$,[17] and $\{Fe_9Re_6\}$[33] congeners, revealed the possibility to induce not only slow magnetic relaxation, but also electron transfer or/and spin crossover assisted single-crystal-to-single-crystal (SCSC) transformations within this cluster topology. A thermally driven phase transition that occurs near 200 K was found to be accompanied by a $^{HS}Fe^{II}$ $W^{V}$ ↔ $^{HS}Fe^{III}$ $W^{IV}$ charge transfer for $\{Fe_9W_6\}$,[17] a double channel charge transfer with Co-centered spin transition lead to a sophisticated $^{HS}Co^{II}$ $^{HS}Fe^{II}$ $W^{V}$ ↔ $^{LS}Co^{III}$ $^{HS}Fe^{III}$ $W^{IV}$ equilibrium in the $\{Fe_6Co_3W_6\}$,[29] while a gradual Fe-centered spin crossover $^{HS}Fe^{II}$ ↔ $^{LS}Fe^{II}$ was detected in the $\{Fe_9Re_6\}$ molecule.[33] By showing the functional potential of such $\{M_9M'_6\}$ molecules, we have outlined a new research path in magnetochemistry of polycyanidometallates. Within our approach, the cyanido-bridged $\{M_9M'_6\}$ cluster can be considered as a specific type of molecular nanosolution in which various types and ratios of metal ions can be controllably inserted into the stable coordination skeleton to tune the compound's properties. We thus exploit the general idea of molecular solid solutions being highly efficient tools for controlling functionalities of molecular materials, such as as magnetic ordering,[34] slow magnetic relaxation,[35] spin crossover,[36] or luminescence.[37] This approach has been already explored successfully in traditional inorganic materials.[38]

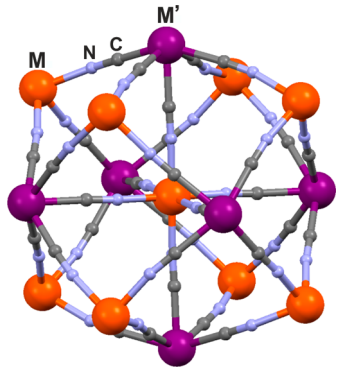


**Figure 1.** Cyanido-bridged core of the $\{M_9M'_6\}$ molecule. M sites can be occupied by 3d metal ions (Mn, Fe, Co, Ni) while M′ centers consist of 4d (Mo) or 5d (W, Re) metal ions.

In this context, we have decided to expand the application of $\{M_9M'_6\}$ clusters in molecular solid solutions in order to take an overall control over their phase transition and SMM functionalities through the adjustment of metal composition. Thus, we present the syntheses and properties of the whole original series of solid state solution materials composed of trimetallic clusters $\{Fe_{9-x}Co_x[W(CN)_8]_6(MeOH)_{24}\}\cdot 12MeOH$ ($x$ = 0, 1, ..., 8, 9; compounds **0**, **1**, ..., **8**, **9**; the integer values of $x$ stands for the approximate amounts obtained from SEM EDS analysis, see SI section Table S2). The series reveals two distinct functionalities, (i) charge transfer assisted reversible structural and spin phase transitions, and (ii) high spin ground state and magnetic anisotropy, which leads to slow magnetic relaxation. The increase of Co content systematically diminishes the charge transfer effects and favors slow magnetic relaxations. These changes of properties, which are related to the metal composition, were precisely investigated by complete structural single crystal and powder X-ray diffraction studies, differential scanning calorimetry (DSC) analysis, temperature variable infrared and $^{57}$Fe Mössbauer spectroscopies, and magnetic measurements.

## RESULTS AND DISCUSSION

**Synthesis and Preliminary Characterization.** The isomorphous and isostructural crystals of $\{Fe_{9-x}Co_x[W(CN)_8]_6(MeOH)_{24}\}\cdot 12MeOH$, **0**−**9**, were prepared according to a


DOI: 10.1021/jacs.5b11924
J. Am. Chem. Soc. 2016, 138, 1635−1646

modification of the method that was previously reported.[17,29] They were grown by mixing $Fe^{II}Cl_2{\cdot}4H_2O$, $Co^{II}Cl_2{\cdot}6H_2O$, and sodium or the tetrabutylammonium salt of $[W^V(CN)_8]^{3-}$ in methanol in a molar ratio that corresponded to the targeted composition (Table S1, for details, see Experimental Section). The crystals of **0**–**9** preserve their morphology, structure, and properties while stored in the mother liquor (**MeOH**), or in Apiezon N grease (**ap**), hence they were characterized in these protectants as **0**–**9@MeOH** or **0**–**9@ap**, respectively. After removal from the mother liquor, they exchange MeOH to $H_2O$ solvent to give the hydrated (**hyd**) residues **0hyd**–**9hyd** of the general composition $\{Fe_{9-x}Co_x[W(CN)_8]_6\}{\cdot}32H_2O$ (Table S1). This was confirmed by IR spectra and elemental analysis. The average Fe:Co:W atomic ratios were determined by X-ray microanalysis using the SEM EDS system to change gradually from ~8:1:6 for **1** to ~1:8:6 for **8**, within the experimental error limits (Table S2). The crystals reveal the identical block shape over the whole series with continuously changing color from deep green for **0** through green-to-brown, brown for **4** and **5**, brown-to-red up to deep red for **9** (Figure 2a). This tendency is followed by the coloration change in the series of freshly prepared mother solutions spawning the crystalline products of **0**–**9@MeOH** (Figure 2b). The corresponding UV–vis–NIR spectra reveal a systematic change tendency with two isosbestic points close to 375 and 600 nm (Figure 2c). The solution spectrum of **0** is strongly reminiscent of the solid state spectra of **0@ap**.[17] The most significant and eye-catching feature of all solution spectra is a strong broad absorption band above 600 nm, interpreted in terms of the complex metal-to-metal charge transfer (MMCT) $Fe^{II}W^V \rightarrow Fe^{III}W^{IV}$ transition within the molecular platform of the Fe-NC-W linkages.[17] This band systematically disappears with the decreasing Fe:Co molar ratio along the **0** to **9** series (Figure 2c). At the same time, the other strong absorption band appears in the spectral range of 375–600 nm, and this band can be assigned to the ligand field (LF) absorption of $^{HS}Co^{II}$ sites and possibly also attributed to the MMCT $Co^{II}W^V \rightarrow Co^{III}W^{IV}$ transition.[13] Below 375 nm the spectra are dominated by the ligand-to-metal charge transfer (LMCT) transitions within $[W(CN)_8]^{n-}$ moieties.[5d,13,17] The above features suggest that $\{Fe_{9-x}Co_x[W(CN)_8]_6\}$ clusters of **0**–**9** are also present in a mother liquor, which is consistent with the previous report for other $\{M_9W_6\}$ clusters.[32b]

**Single Crystal X-ray Diffraction Studies.** The precise single XRD measurements were performed on **0**–**8@ap** samples both at 250 and 130 K in order to obtain the detailed structural data that represents the high temperature (HT) and low temperature (LT) phases, respectively (Tables S3–S7, Figures 3, and S1–S2). For the sake of simplicity, the identical atom numbering scheme was applied to all crystal structures (Figure 3a). The crystal structures of **0**–**8** were solved and refined in the monoclinic $C2/c$ space group and are composed of pentadecanuclear cyanido-bridged MeOH-protected clusters of body-centered six capped cubic topology, and crystallized MeOH molecules. The asymmetric units contain a half of central M1 unit and four external M2–M5 units, joined by three $[W1–W3(CN)_8]^{3-}$ units. The comparison of mean M–L distances in HT and in LT gives the significant relative change of M–L bondlengths, $\Delta$(M–L) indicating the presence of the structural HT → LT phase transition (Figure 3b). The strongest tendency change is observed for the central M1 site, and reveals the bell shape. The maximum change exceeding 7% is achieved for $x = 3$ and 4 (compounds **3** and **4**), while a significant change close to 6% is seen for $x = 2$ and 5 (compounds **2** and **5**). The generally

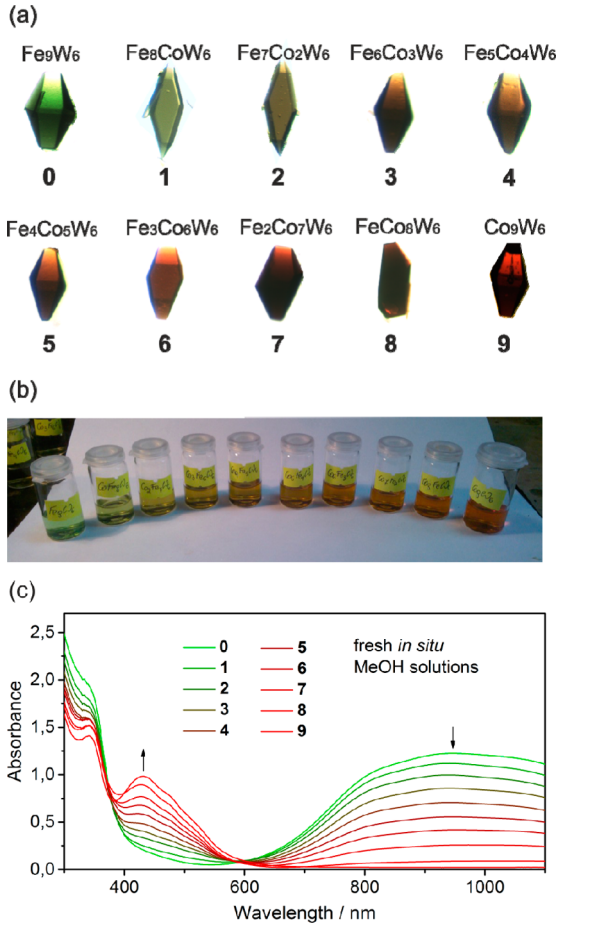


**Figure 2.** Photographs of single crystals of **0**–**9@MeOH** together with the compounds numbering code (a), the photographs of freshly prepared methanolic solutions of reactants in the proper $Fe^{II}$:$Co^{II}$:$W^V$ molar ratio (b), and the relevant electronic absorption spectra, (concentration of $[W(CN)_8]^{3-}$: 2.4 mM; total concentration of $CoCl_2$ and $FeCl_2$: 3.6 mM) (c).

weaker, anisotropic tendency was observed at M2–M5 positions. Two positions, M2 and M4, show relatively larger $\Delta$(M–L) compared to the positions M3 and M5 for iron rich congeners, $x = 1–3$. The maxima of $\Delta$(M–L) were detected for $x = 0–4$ that are 3–4% for M2 and M4 sites, and less than 3% for M3 and M5 sites. They are gradually smaller for **5** and **6**, and for $x = 7$ the $\Delta$(M1–L) remains only on the level of 2%, while $\Delta$(M2–M5/L) becomes negligible. The detailed individual trends of average M–L distances, $d$(M–L), in 250 K and in 130 K are shown in Figure S1, and collected in Tables S6–S7.

Intuitively, the large $\Delta$(M–L) should be interpreted in terms of the possible $^{HS}Co^{II} \rightarrow {}^{LS}Co^{III}$ charge transfer induced spin transition (CTIST) or $^{HS}Fe^{II} \rightarrow {}^{LS}Fe^{II}$ spin crossover (SCO) process. The $\Delta$(M–L) changes grow with the increasing amount of Co on going from **0** to **4** which suggests that they are related to the Co–W equilibrium. This is also supported by the $^{HS}Co^{II}W^V \rightarrow {}^{LS}Co^{III}W^{IV}$ spin-phase transitions observed recently for the series of $Co^{II}$-$[W^V(CN)_8]^{3-}$ compounds.[13] It is also in agreement with the results of spectroscopic and magnetic data presented hereafter. The last plausible option is the $Fe^{II}$-centered SCO observed by us recently in $\{Fe_9Re_6\}$ clusters;[33] however, in this case it is generaly disfavored (*see the discussion below*). Thus, we suggest that M1 sites as well as some of M2 and M4 sites are prone to host the $^{HS}Co^{II} \rightarrow {}^{LS}Co^{III}$ process over the series.


DOI: 10.1021/jacs.5b11924
J. Am. Chem. Soc. 2016, 138, 1635–1646

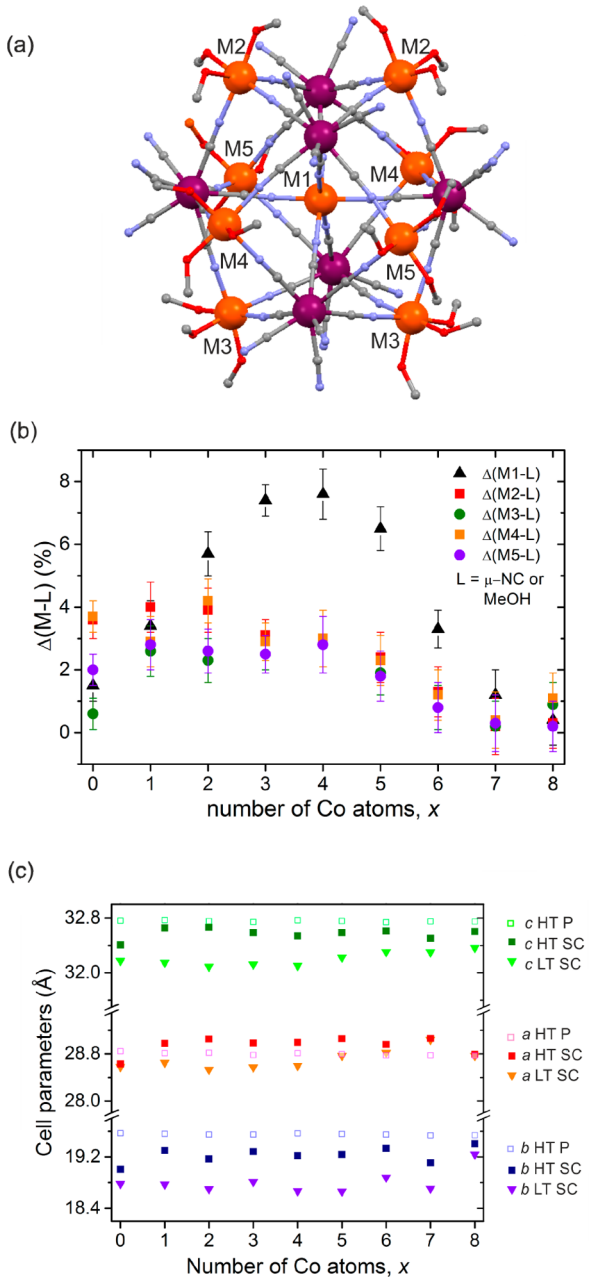


**Figure 3.** Single crystal study of structural phase transition in **0**–**8**: (a) molecular structure with the 3d metal ion M1–M5 (M = Co or Fe) numbering scheme, (b) the mean changes of the M–L distances, Δ(M–L), (L = $O_{MeOH}$, $N_{CN}^-$) in different 3d metal ion sites, and (c) the changes in crystal cell parameters *a*, *b* and *c*. Notations: HT P, powder data at 293 K; HT SC, single crystal data at 250 K; LT SC, single crystal data at 130 K.

The remaining sites including M3 and M5 should rather host the accompanying $^{HS}Fe^{II} \rightarrow {}^{HS}Fe^{III}$ change. Tables S6 and S7 indicate the proposed occupancy of particular M1–M5 sites, basing on the values of Δ(M–L).

The significant local structural changes observed for congeners **1**–**6** are accompanied by the visible changes in the unit cell parameters (Figure 3c). As the natural consequence of the dramatic decrease in bondlengths, the lattice constants are also strongly decreased on going from HT to LT phases. In addition, the trends of changes in cell parameters with increasing *x* illustrate a directional character of phase transitions (Figure 3c, Figure S2). The period *c* and the period *b* change visibly along the whole series **0**–**8**, while the period *a* is significantly modified only for **0**–**5**. These observations are in line with the results obtained using all other techniques in this work, and can be interpreted in terms of diverse intercluster contacts in this directions, and different flexibility of M2, M3 and M4 sites. The thermal dependence of coordination bond lengths and lattice constants in **0**–**8** show that the phase transition is mainly observed for **0**–**5**, and later gradually disappears for **6**–**8**. This proves that the phase transition has to be promoted by $^{HS}Fe^{II}W^{V} \rightarrow {}^{HS}Fe^{III}W^{IV}$ electron transfer as is observed even for congener **0** without the participation of Co ions. It occurs in **0** only with the moderate changes in the molecular structure of the cluster due to the limitations imposed by the difference of ionic radii of $^{HS}Fe^{II}$ and $^{HS}Fe^{III}$. The introduction of $Co^{2+}$ ions enables the significant changes in the molecular structure in **1**–**5** due to the $^{HS}Co^{II}W^{V} \rightarrow {}^{LS}Co^{III}W^{IV}$ process supported by $^{HS}Fe^{II}W^{V} \rightarrow {}^{HS}Fe^{III}W^{IV}$ process. The further replacement of $Fe^{2+}$ by $Co^{2+}$ ions leads to the systematic suppression of molecular changes and structural phase transitions.

**Powder X-ray Diffraction and Calorimetric Studies.** The further characterization of phase transitions in **0**–**9@MeOH** involved variable temperature powder X-ray diffraction (PXRD) measurements in the 293–140 K range, both during cooling and subsequent heating. All compounds in the **0**–**9** series are isostructural at $T$ = 293 K giving analogous powder diffractograms consistent with the monocrystalline data. The slight compression of the unit cell with increasing *x*, from **0** to **9**, is consistent with the systematic replacement of Fe ions by Co ion, due to shorter metal–ligand bond lengths of $^{HS}Co^{II}$ complexes compared to $^{HS}Fe^{II}$ complexes (Figure 4a).[29] Powder diffractograms present clearly the unique series of fully reversible structural phase-transitions in **0**–**5**. The critical temperatures $T_{\downarrow}^{PXRD}$ and $T_{\uparrow}^{PXRD}$ can be read from thermal evolution of the selected PXRD peak (~11° 2$\theta$) attributed to (2 2–1) and (2 0–4) reflections (Figure 4b; Figure S3, Figure S4 and Figure S5). A recognizable shift in the transition temperatures toward lower temperatures with the increased number of Co ions is observed. Compounds **0**–**3** reveal the abrupt transitions, within less than 5 K temperature range, with the maximum amplitude of 2$\theta$ peak position over the series, whereas compounds **4** and **5** reveals a systematic suppression of this amplitude and diffusion over the 2$\theta$ scale. Finally, **6**–**8** do not show any transition in the examined temperature range, revealing only the standard thermal compression with decreasing temperature. Interestingly, the average transition temperatures for **0**–**4** are found to be an approximately linear function of the number of iron sites suggesting that the amount of Fe–W CT pairs in the cluster core is the dominating factor in the thermal induction of the phase transition (Figure 4b, Figure S6). These data are in a good agreement with the calorimetric studies, and magnetic data measured for **0**–**9@MeOH**.

Differential scanning calorimetry (DSC) measurements for **0**–**3** show sharp heat flow peaks indicating the occurrence of first order phase transitions (Figure 4c). For **4** and **5** the systematic broadening was noted. For **6**–**8** no signature of structural phase transition was found. The critical temperatures $T_{\downarrow}^{DSC}$ and $T_{\uparrow}^{DSC}$ coincide perfectly with $T_{\downarrow}^{PXRD}$ and $T_{\uparrow}^{PXRD}$ (Table S8). The thermodynamic parameters, change of the enthalpy Δ$H$ and entropy Δ$S$ for the **0**–**3** were calculated for $T_{\downarrow}^{DSC}$ assuming the zero value of Gibbs free energy, Δ$G$ = 0. $Fe_9W_6$, **0**, reveals the significant values of 62(4) kJ·mol$^{-1}$ for Δ$H$ and 300(20) J·K$^{-1}$·mol$^{-1}$ for Δ$S$. The gradual exchange of Fe by Co on going


DOI: 10.1021/jacs.5b11924
J. Am. Chem. Soc. 2016, 138, 1635–1646

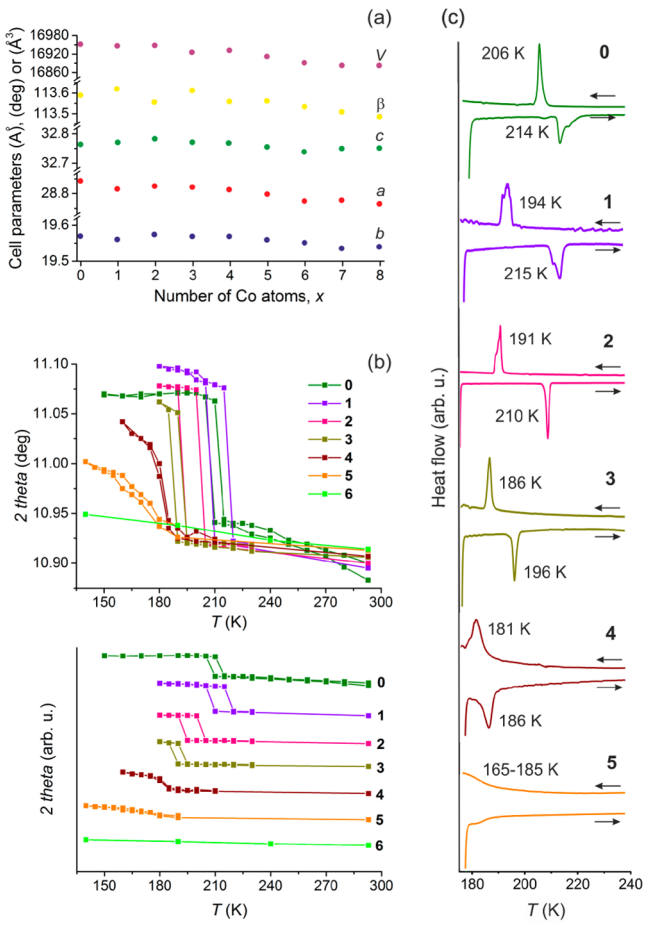


**Figure 4.** Powder X-ray diffraction (PXRD) and differential scanning calorimetry (DSC) studies of structural phase transitions in **0–9@MeOH**: (a) the cell parameters for **0–8** at room temperature, (b) thermal evolution of the selected diffraction peak position in HT phase → LT phase → HT phase sequence of **0–6**, and (c) DSC curves in HT phase → LT phase → HT phase sequence of **0–5** (heat flow, scan rate of 10 K·min$^{-1}$).

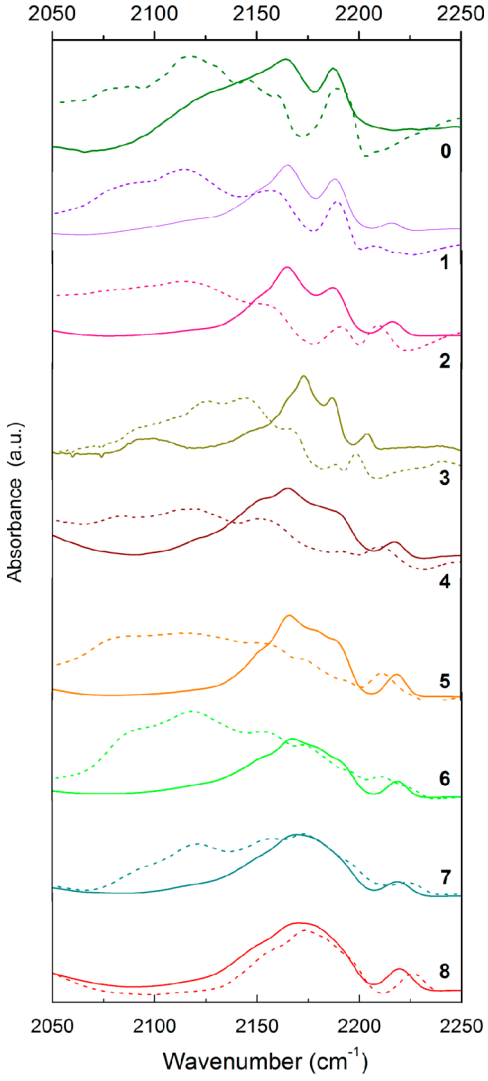


**Figure 5.** Infrared spectra for solids **0–8@ap** at 293 K, (HT, solid lines) and at 130 K (LT phase, dashed lines).

from **0** to **1–3** induce the further increase of thermodynamic parameters. Going from **0** to **1**, $\Delta H$ increases to 78(16) kJ·mol$^{-1}$, and $\Delta S$ to 405(84) J·K$^{-1}$·mol$^{-1}$ which suggests that the $^{HS}Co^{II}$ $W^{V}$ ↔ $^{LS}Co^{III}$ $W^{IV}$ CTIST process is responsible for the higher enthalpy and entropy change than the $Fe^{II}$ $W^{V}$ ↔ $Fe^{III}$ $W^{IV}$ CT which can be also correlated with the larger changes in bond lengths (Figure 3), and more pronounced changes in spin values for complex Co–W CTIST than simple Fe–W electron transfer. The exchange of the next Fe by Co, in **2**, results in a further increase of the thermodynamic parameters to $\Delta H$ = 101(11) kJ·mol$^{-1}$ and $\Delta S$ = 528(60) J·K$^{-1}$·mol$^{-1}$, due to the increasing number of CT-active Co-NC-W linkages. The further incorporation of third Co site in the cluster in **3** leads to the values $\Delta H$ = 105(40) kJ·mol$^{-1}$ and $\Delta S$ = 565(200) J·K$^{-1}$·mol$^{-1}$, which makes for a smaller relative increase compared to the former cases. This suggests that, despite the increasing Co/Fe ratio, the number of CT-active Co–W linkages does not increase significantly. Due to partial overlapping with the DSC peak related to the liquid–solid phase transition of methanol, the thermodynamic parameters for **4** and **5** could not be reliably determined.

**Spectroscopic Data.** The phase transitions were followed by IR spectroscopy in the range of stretching vibrations of cyanides, $\nu$(CN) (Figures 5; Figure S7, Figure S8, Table S9). This region is frequently used in the discrimination between $W^{V}$ and $W^{IV}$ oxidation states of $[W(CN)_8]^{n-}$, due to the different energies of the $\nu$(CN) transitions as they are related to the rearrangement of electronic density along 5d(W)-$\pi$*(CN) orbital system.[39,13] Room temperature spectra of trimetallic congeners **1–8@ap** showed absorption bands in the range of 2140–2225 cm$^{-1}$, which suggests the domination of the $W^{V}$ valence state in both terminal and bridging $[W(CN)_8]^{3-}$ anions. Low temperature spectra of **0–7** reveal a significant change in the whole $\nu$(CN) range, featuring the additional absorption band in 2075–2140 cm$^{-1}$ range. This is interpreted in terms of coexistence of $W^{V}$ and $W^{IV}$ valences, reminiscent for the $W^{V}$ → $W^{IV}$ electron transfer process. Conversely to that, the congener **8** does not show absorption below 2140 cm$^{-1}$ indicating the tendency to suppress the electron transfer and probably the phase transition, in line with the structural data. The detailed thermal evolution of IR spectra illustrates conveniently the temperature ranges of the relevant spectral changes, typically in range 220–180 K for $T_{\downarrow}^{IR}$ and 220–250 K for of $T_{\uparrow}^{IR}$ (Figure S7, Figure S8, Table S9). These ranges do not converge exactly with the phase transition temperatures, which suggest that the changes in electronic structure do not coincide exactly with the phase transition.


DOI: 10.1021/jacs.5b11924
J. Am. Chem. Soc. 2016, 138, 1635–1646

The results are in agreement with the previous observation for $\{Fe_6Co_3W_6\}$;[29] however, they are in contrast with the behavior of $\{Fe_9W_6\}$,[17] where the temperature ranges are 270−215 K for $T_{\downarrow}^{IR}$ K and 230−298 for $T_{\uparrow}^{IR}$. This indicates a significantly different character of **0** compared to the whole trimetallic series.

The phase transitions for iron-rich **0−4@ap** solids were also examined between 80 and 297 K by $^{57}$Fe Mössbauer spectroscopy. The thermal evolution of spectra together with the fitted components is visualized in Figure S9. The detailed analysis of spectra, including the consideration of distinguished temperature dependence of the Debye−Waller factor for $^{HS}Fe^{II}$ and $^{HS}Fe^{III}$, allowed the determination of the iron spin states composition (Figure S10, Table S10−S16). The phase transition is nicely illustrated by the thermal dependence of $^{HS}Fe^{II}$ molar fraction $\gamma_{(HS)Fe(II)}$ (Figure 6). For **1−4** only the $^{HS}Fe^{II}$ spin state at 297 K

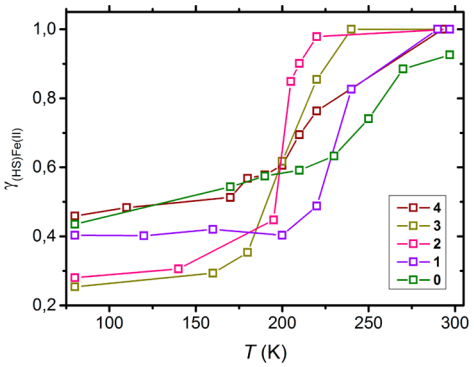


**Figure 6.** Thermal dependence of $^{HS}Fe^{II}$ molar fraction, $\gamma_{(HS)FeII}(T)$, for **0−4** determined by $^{57}$Fe Mössbauer effect spectroscopy.

is present, as the spectra were easily deconvoluted into 2 doublets (reflecting the tiny difference in the local coordination of the Fe ions) with the parameters unambiguously assigned to this Fe state. Upon cooling, these compounds undergo relatively sharp transitions in temperature ranges significantly below the room temperature, tending to the stable LT composition below 190 K. This is manifested by the appearance and systematic growth of doublets which are assignable to $^{HS}Fe^{III}$. These results suggest that the local electron configuration is reorganized at temperatures slightly above the temperatures of the structural transitions, in good agreement with IR spectra. Conversely to that, compound **0** at 297 K shows the coexistence of the $^{HS}Fe^{II}$ spin state with the $^{HS}Fe^{III}$ spin state (ca. 7%). Compared to **1−4**, the $^{HS}Fe^{II}$ states disappears more gradually with decreasing temperature, resulting in a stable configuration below ca. 170 K that is accompanied by the appearance of $^{HS}Fe^{III}$ instead. However, for the sake of reliable quantitative analysis of magnetic data (*see below*), we are inclined to consider here also the fractional appearance of $^{LS}Fe^{II}$ state occurring statistically along the whole molecular network of solid **0** (Figure 3, Table S11). This is in line with our most recent results for $\{Fe_9Re_6\}$ clusters,[33] where a classical gradual $Fe^{II}$-centered SCO appeared in the M1 site. Due to the inherent uncertainty of discrimination between $^{LS}Fe^{II}$ and $^{HS}Fe^{III}$ spin states by Mössbauer spectroscopy, the full interpretation of the spectra were supported by the results of magnetic measurements. Thus, these data are further discussed in the next section devoted to magnetic properties.

**Magnetic Measurements.** The magnetic properties of **0−9** were measured for samples immersed in MeOH. The $\chi T(T)$ plot, together with the zoomed data for samples **0−5** in the transition regions, is presented in Figure 7. The gradual change of

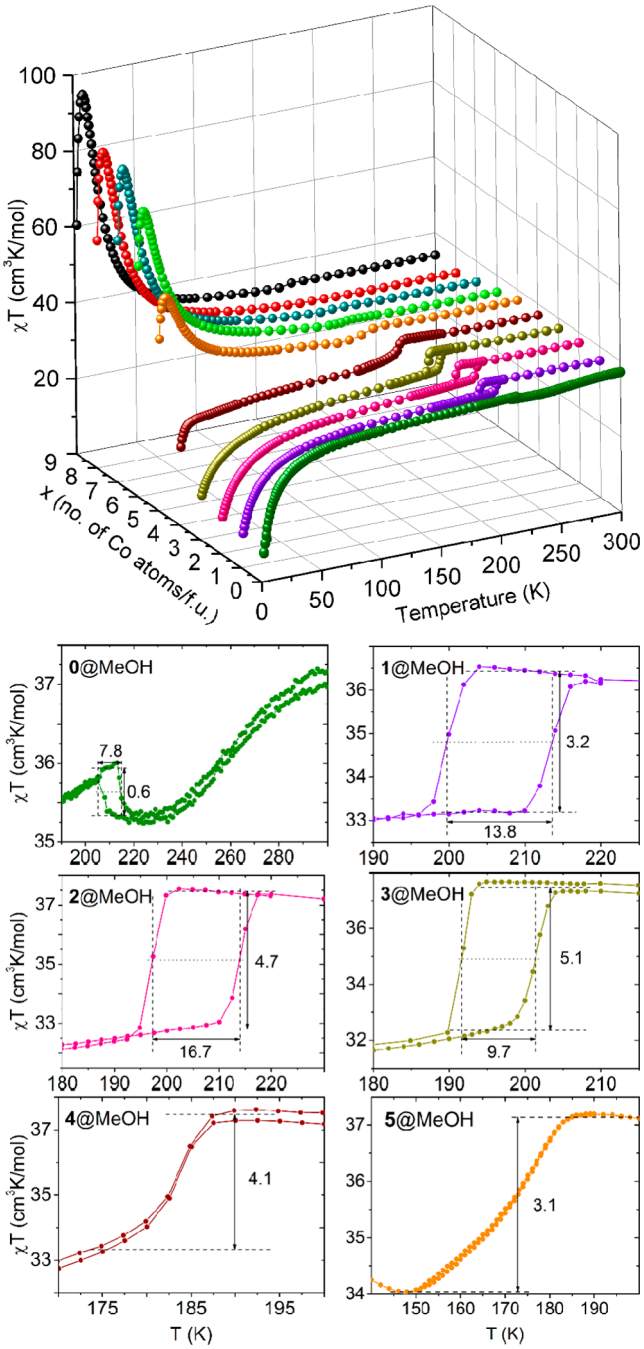


**Figure 7.** $\chi T(T)$ plot for samples **0−9@MeOH** (top) with zoomed thermal hystereses regions for samples **0−5** (bottom). The solid lines are to guide the eye. Note the difference in the vertical scale for **0**, compared to **1−5**.

the magnetic behavior with the change of stoichiometry is observed and shall be discussed in a variety of aspects.

First, the $\chi T$ values at room temperature tend to decrease slowly yet systematically with an increasing amount of Co, $x$, from 37.0 to 33.1 $cm^3 \cdot K \cdot mol^{-1}$, for **0** and **9**, respectively. This is consistent with the expected trends, assuming the following single ion parameters: $S_{Fe(II)} = 2$ and $g_{Fe(II)} = 2.3$ for $^{HS}Fe^{II}$,[40a] $S_{Fe(III)} = 5/2$ and $g_{Fe(III)} = 2.0$ for $^{HS}Fe^{III}$,[40b] $S_{W(V)} = 1/2$ and $g_{W(V)} = 2.0$ for $W^{V}$,[13b] and $S_{Co(II)} = 3/2$ and $g_{Co(II)} = 2.7$ for $^{HS}Co^{II}$.[40c]

Second, it is clearly visible that the behavior of the samples at higher temperatures (180−300 K) is nontrivial, mostly due to


DOI: 10.1021/jacs.5b11924
J. Am. Chem. Soc. 2016, 138, 1635−1646

**Table 1. Spin/Oxidation State Compositions for HT Phases, LT Phases and the Respective Intermediate Phases of 0−4 Including the Comparison of Experimental and Theoretical Values of $\Delta\chi T$ Amplitude of Thermal Hysteresis**

| compound | $T$/K | composition | $\Delta\chi T$ calculated ($cm^3$ K/mol) | $\Delta\chi T$ experimental ($cm^3$ K/mol) |
|---|---|---|---|---|
| **0** | 295 | $(^{HS}Fe^{III})_{0.67}(^{HS}Fe^{II})_{8.32}(^{LS}Fe^{II})_{0.01}(W^{V})_{5.33}(W^{IV})_{0.67}$ | −0.64 | −0.66 |
| | 230 | $(^{HS}Fe^{III})_{2.87}(^{HS}Fe^{II})_{5.65}(^{LS}Fe^{II})_{0.48}(W^{V})_{3.13}(W^{IV})_{2.87}$ | | |
| | 210 | $(^{HS}Fe^{III})_{3.38}(^{HS}Fe^{II})_{5.31}(^{LS}Fe^{II})_{0.31}(W^{V})_{2.62}(W^{IV})_{3.38}$ | | |
| **1** | 295 | $(^{HS}Fe^{II})_{8}(^{HS}Co^{II})_{1}(W^{V})_{6}$ | 2.6 | 3.2 |
| | 240 | $(^{HS}Fe^{III})_{1.36}(^{HS}Fe^{II})_{6.64}(^{HS}Co^{II})_{1}(W^{V})_{4.64}(W^{IV})_{1.36}$ | | |
| | 200 | $(^{HS}Fe^{III})_{4.80}(^{HS}Fe^{II})_{3.20}(^{HS}Co^{II})_{0.56}(^{LS}Co^{III})_{0.44}(W^{V})_{0.76}(W^{IV})_{5.24}$ | | |
| | 160 | $(^{HS}Fe^{III})_{4.64}(^{HS}Fe^{II})_{3.36}(^{HS}Co^{II})_{0.30}(^{LS}Co^{III})_{0.70}(W^{V})_{0.66}(W^{IV})_{5.34}$ | | |
| **2** | 295 | $(^{HS}Fe^{II})_{7}(^{HS}Co^{II})_{2}(W^{V})_{6}$ | 3.5 | 4.7 |
| | 220 | $(^{HS}Fe^{III})_{0.15}(^{HS}Fe^{II})_{6.85}(^{HS}Co^{II})_{2}(W^{V})_{5.85}(W^{IV})_{0.15}$ | | |
| | 200 | $(^{HS}Fe^{III})_{3.87}(^{HS}Fe^{II})_{3.13}(^{LS}Co^{III})_{1.65}(^{HS}Co^{II})_{0.35}(W^{V})_{1.78}(W^{IV})_{4.22}$ | | |
| | 140 | $(^{HS}Fe^{III})_{4.86}(^{HS}Fe^{II})_{2.14}(^{LS}Co^{III})_{0.96}(^{HS}Co^{II})_{1.04}(W^{V})_{0.18}(W^{IV})_{5.82}$ | | |
| **3** | 295 | $(^{HS}Fe^{II})_{6}(^{HS}Co^{II})_{3}(W^{V})_{6}$ | 5.1 | 5.1 |
| | 220 | $(^{HS}Fe^{III})_{0.87}(^{HS}Fe^{II})_{5.13}(^{HS}Co^{II})_{3}(W^{V})_{5.13}(W^{IV})_{0.87}$ | | |
| | 180 | $(^{HS}Fe^{III})_{3.88}(^{HS}Fe^{II})_{2.12}(^{LS}Co^{III})_{1.0}(^{HS}Co^{II})_{2.0}(W^{V})_{1.12}(W^{IV})_{4.88}$ | | |
| | 160 | $(^{HS}Fe^{III})_{4.24}(^{HS}Fe^{II})_{1.76}(^{LS}Co^{III})_{1.38}(^{HS}Co^{II})_{1.62}(W^{V})_{0.26}(W^{IV})_{5.74}$ | | |
| **4** | 295 | $(^{HS}Fe^{II})_{5}(^{HS}Co^{II})_{4}(W^{V})_{6}$ | 4.1 | 4.1 |
| | 200 | $(^{HS}Fe^{III})_{1.97}(^{HS}Fe^{II})_{3.03}(^{HS}Co^{II})_{4}(W^{V})_{4.03}(W^{IV})_{1.97}$ | | |
| | 180 | $(^{HS}Fe^{III})_{2.16}(^{HS}Fe^{II})_{2.84}(^{LS}Co^{III})_{0.90}(^{HS}Co^{II})_{3.10}(W^{V})_{2.94}(W^{IV})_{3.06}$ | | |
| | 170 | $(^{HS}Fe^{III})_{2.44}(^{HS}Fe^{II})_{2.56}(^{LS}Co^{III})_{1.10}(^{HS}Co^{II})_{2.90}(W^{V})_{2.46}(W^{IV})_{3.54}$ | | |

the emergence of reversible phase transitions with a thermal hysteresis near 200 K for the Fe rich phases **0**−**3**. The hysteresis is almost suppressed for **4**, however, the phase transition is still evident. The small remnant phase transition is still visible for sample **5**, and disappears completely for the Fe poor crystals of **6**−**9**. The existence of the thermal hysteresis, and the values of the respective $T_{\downarrow}$ and $T_{\uparrow}$ are consistent with the results of the DSC measurements, and those of the PXRD studies (Table S8).

The analysis of the $\chi T$ values at room temperature for the aforementioned samples shall be directly connected with the detailed analysis of the spin transition. To achieve this, reliable overall oxidation/spin state compositions were proposed, based on the combined results of $^{57}$Fe Mössbauer spectroscopy and single-crystal XRD studies and assuming the occurrence of $^{HS}Fe^{II}W^{V} \rightarrow {}^{HS}Fe^{III}W^{IV}$ and $^{HS}Co^{II}W^{V} \rightarrow {}^{LS}Co^{III}W^{IV}$ processes. As a result, Table 1 shows the compositions at crucial temperature points, including the temperatures limiting the hysteresis. Then, the compositions were used to estimate the expected theoretical values of $\Delta\chi T$ amplitude and compared to the observed experimental values. The single ion parameters of $^{HS}Fe^{II}$, $^{HS}Fe^{III}$, $W^{V}$ and $^{HS}Co^{II}$ were assumed as above, while the zero contributions to the paramagnetic moment were assumed for the diamagnetic $W^{IV}$, $^{LS}Fe^{II}$ and $^{LS}Co^{III}$ centers. A reasonable agreement was achieved between the expected and observed $\Delta\chi T$ at hysteresis. Thus, we infer that the proposed $^{HS}Fe^{II}W^{V} \rightarrow {}^{HS}Fe^{III}W^{IV}$ and $^{HS}Co^{II}W^{V} \rightarrow {}^{LS}Co^{III}W^{IV}$ processes, i.e., the electron charge transfer from 3d elements to 5d tungsten, explain well the observed behaviors.

In the case of **0**, an unusual shape of the $\chi T(T)$ should be reconsidered, compared with the previous analysis done based on the $^{57}$Fe Mössbauer data measured only for RT and 80 K.[17] A small yet apparent decrease of the signal, ca. 1.6 $cm^3 \cdot K \cdot mol^{-1}$ on going from 293 to 220 K, preceding the structural transition, is now reinterpreted in terms of the simultaneous run of $^{HS}Fe^{II} \rightarrow {}^{III}Fe^{HS}$ CT, and the fractional $^{HS}Fe^{II} \rightarrow {}^{LS}Fe^{II}$ process. The latter occurs most probably at the central M1 site in some of the clusters. This is supported by our most recent research on the $Fe_9Re_6$ congener.[33] Moreover, the diffused character, and the range of 293−220 K are strongly reminiscent for the Fe-centered SCO processes observed for several cyanido-bridged molecular systems.[8e,16] We also believe that this fractional transition, by the absence of $^{HS}Co^{II} \rightarrow {}^{LS}Co^{III}$, assures the strong local structural changes and, thus, facilitate the structural phase transition below 220 K. Last, but not least, it is required for a good agreement between the expected and observed values of $\Delta\chi T$.

Third, the low temperature behavior of $\chi T$ below the phase transition undergoes apparent systematic modifications, confirming the presence of the two distinct $x$ regions. For **0**−**3** $\chi T$ decrease smoothly down to ca. 50 K, then they decrease more rapidly to reach the value of ca. 15−20 $cm^3 \cdot K \cdot mol^{-1}$. This behavior can be interpreted mainly in terms of single ion properties of the remaining paramagnetic ions. Plausible antiferromagnetic coupling is strongly limited due to the excess of diamagnetic $[W^{IV}(CN)_8]^{4-}$ over the paramagnetic $[W^{V}(CN)_8]^{3-}$ ions. This tendency evidently breaks between the congeners **4** and **5**, the latter one showing the phase transition accompanied by an increase of $\chi T$ with decreasing $T$ and the maximum at $T$ ca. 10 K. For **6**−**8** the $\chi T$ signals increase monotonically, and show that the maximum increases with growing $x$. The appearance of the maximum is reminiscent of the ferromagnetic interaction $^{HS}Co^{II}$−$W^{V}$ observed in $\{Co_9W_6\}$ clusters,[28b,32] and other polynuclear $Co^{II}$-$[W^{V}(CN)_8]^{3-}$ assemblies.[5d,41] The overall gradual rise of the $\chi T(T)$ signals at low temperatures is confirmed by isothermal $M(H)$ curves measured at 1.8 K (Figure S11). They could be divided into two sets: those for the **5**−**9** solids start to saturate at lower values of the magnetic field, and reach higher values of magnetization compared to those of **0**−**4**. Thus, the $M(H)$ curves confirm the high spin character of the clusters in **5**−**9**, as the significant $Co^{II}$−$W^{V}$ ferromagnetic interactions start to contribute.

AC magnetic measurements versus temperature showed a significant frequency dependence and nonzero $\chi''$ for samples **5**−**9** (Figure 8a) revealing the other important aspect of the magnetic behavior of the clusters on this side of the stoichiometric spectrum. It is clearly visible that larger concentration of Co implies more prominent frequency dependence. AC magnetic susceptibility becomes gradually frequency independent with the increasing Fe concentration. These results prompted detailed AC susceptibility versus frequency measurements at a


DOI: 10.1021/jacs.5b11924
J. Am. Chem. Soc. 2016, 138, 1635−1646

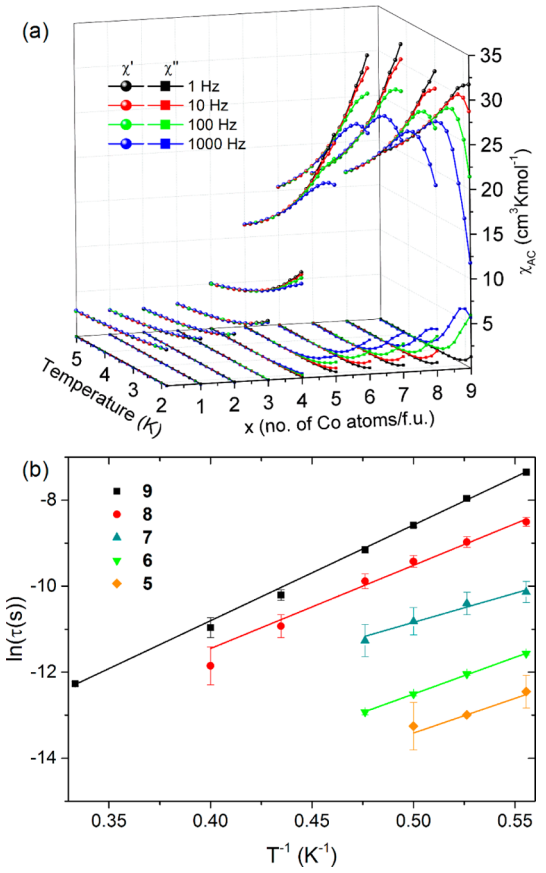


**Figure 8.** (a) Alternate-current (*ac*) magnetic susceptibilities measured at $H_{AC}$ = 3 Oe and $f_{AC}$ = 1, 10, 100, and 1000 Hz versus temperature for samples **0**–**9**. The solid lines are to guide the eye. (b) A plot of ln($\tau$) obtained from the Cole–Cole fits as a function of inverse temperature with respective linear fits of the Arrhenius law (solid lines).

series of temperatures to investigate the possible SMM behavior of the clusters (Figure S12). The first observation is that these measurements are consistent with the AC susceptibility versus temperature measurements—the peaks in $\chi''$ are well visible for the samples with the highest concentrations of Co. This was expected as $Co^{II}$ centers possess a large single-ion anisotropy which is the necessary condition for slow magnetic relaxations to appear.[19] With the decreasing amount of $Co^{II}$ the aforementioned peaks shift toward higher frequencies and grow smaller in signal. Where possible, the data were then fitted simultaneously with the Cole–Cole model, $\chi'$ and $\chi''$:

$$\chi(\omega) = \chi_S + \frac{\chi_T - \chi_S}{1 + (i\omega\tau)^{1-\alpha}}$$

where $\chi = \chi' - i\chi''$ is the complex susceptibility, $\chi_T$ and $\chi_S$ are isothermal and adiabatic susceptibilities, respectively, $\tau$ is the average relaxation time, and $\alpha$ is the parameter describing the distribution of the relaxation times. The relaxation times obtained from the Cole–Cole fits were then fitted with the Arrhenius law (Figure 8b).

The $\alpha$ parameters, together with the values of prefactor $\tau_0$ and the energy barriers obtained from the Arrhenius law fits for **5**–**9** are summarized in Table 2. The large values of $\alpha$ parameters suggest a wide distribution of the relaxation times for **9** that gradually widens further with the decreasing amount of Co in the cluster. A tendency of the energy barrier to take lower values with decreasing Co concentration should be noticed.

**Table 2. Summary of the Parameters from the Cole–Cole Fits for 5–9**

| compound | $\alpha$ | $\tau_0$ (s) | $\Delta E_\tau/k_B$ (K) |
|---|---|---|---|
| **9** | 0.14–0.51 | $3 \times 10^{-9}$ | 22.3(0.3) |
| **8** | 0.47–0.59 | $5 \times 10^{-9}$ | 19.4(1.2) |
| **7** | 0.57–0.65 | $2 \times 10^{-8}$ | 13.7(1.7) |
| **6** | 0.64–0.68 | $7 \times 10^{-10}$ | 17.1(0.3) |
| **5** | 0.68–0.71 | $5 \times 10^{-10}$ | 16.1(3.8) |

## DISCUSSION AND CONCLUSIONS

A fascinating novel series of solid state solutions based on $\{Fe_{9-x}Co_xW_6\}$ clusters exhibit an unprecedented tuning of their properties by the adjustment of 3d metal ion composition, represented by $x$ (Figure 9). It was achieved through a

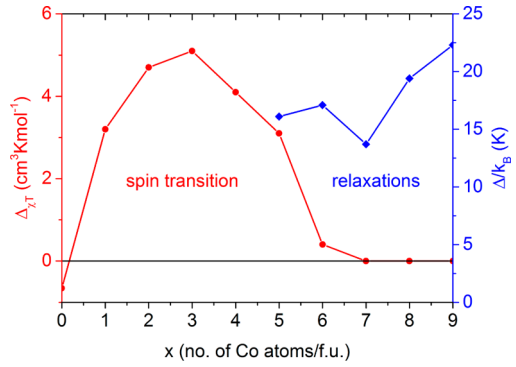


**Figure 9.** Tuning of magnetic properties in the $\{Fe_{9-x}Co_xW_6\}$ series by the number $x$ of Co atoms. The phase transition is represented by the change of magnetic signal, $\Delta_{\chi T}$, while the slow magnetic relaxation is represented by the value of the related energy barrier, $\Delta E$.

stoichiometrically controlled embedding of $Fe^{II}$ and $Co^{II}$ ions at specific sites of a pentadecanuclear $\{Fe_{9-x}Co_xW_6\}$ coordination skeleton. The iron rich phases, $x$ = 0–5 (**0**–**5**), show reversible structural phase transitions in the 160–220 K range. In each case, the phase transition is accompanied by significant changes in the electronic structure of the coordination moieties and occurs with electron transfer along either the Fe-NC-W linkage (phase **0**) or simultaneously within both the Fe-NC-W and Co-NC-W linkages (**1**–**4**). The transition temperatures $T_\downarrow$ and $T_\uparrow$ are shifted almost linearly toward lower temperatures with increasing $x$, keeping the first order character up to $x$ = 4. The coerciveness is lost for **4**, while for the phase **5** ($x$ = 5) the $\chi T$ change with temperature becomes diffuse. On the second side of the composition scale $x$, the cobalt rich phases, $x$ = 5–9 (**5**–**9**), reveal slow magnetic relaxation. This feature becomes more pronounced with increasing $x$, and subsequently the energy barrier also grows on going from **5** to **9**. As a result, phase **5** combines both types of magnetic functionalities.

It is worth discussing in detail the role of the 3d ions in the observed behavior. The Fe-NC-W linkages do activate both the coordination skeleton and the whole molecular network toward the phase transition. We rationalize it by considering the favoring redox potentials of $Fe^{3+}/Fe^{2+}$ in the appropriate ligand environment, and the $[W^V(CN)_8]^{3-}/[W^{IV}(CN)_8]^{4-}$ redox couples. This is confirmed by the presence of $Fe^{3+}$ in pure iron phase **0** at room temperature as well as by the changes of IR and $^{57}$Fe Mössbauer characteristics for **1**–**4**, preceding the transitions in the cooling mode. It was shown that ca. five electrons are transferred from Fe to W centers, going from RT to 80 K. This


DOI: 10.1021/jacs.5b11924
J. Am. Chem. Soc. 2016, 138, 1635–1646

tendency is broken for phase **4**, where only ca. 2.7 Fe per 5 centers are oxidized. This results in the decrease in the cooperativity and loss of hysteretic character. Such a tendency is even strengthened in further members of the family, as we observe diffused bulk transition for **5**, and even transition with the reduced dimensionality of structural changes for **6**, **7** and **8**. On the other hand, the incorporation of $Co^{II}$ significantly tunes the flexibility of the whole system. The introduction of even one $Co^{II}$ center precludes the changes in the Fe spin state at RT, leading to the $\{^{HS}Fe^{II}{}_8{}^{HS}Co^{II}W^{V}{}_6\}$ state at RT (**1**$^{HT}$) without any sign of charge or electron transfer. The further addition of $Co^{II}$ promotes this tendency once more, giving $\{^{HS}Fe^{II}{}_{9-x}{}^{HS}Co^{II}{}_xW^{V}{}_6\}$ phases. Moreover, the onset of changes in the IR and Mössbauer characteristics related to $Fe^{II}W^{V} \rightarrow Fe^{III}W^{IV}$ process was moved to significantly lower temperatures compared to **0**, while the $^{HS}Fe^{II} \rightarrow {}^{LS}Fe^{II}$ transition that is present in **0** was canceled. At the same time, the $Co^{2+}$ ions contribute strongly to the change of magnetic moment in the hysteresis region, starting from compound **1** with a single Co-NC-W linkage. Such behavior is continued in phases **2**−**4**. We believe that this is achieved due to the active Co−W electronic isomerism that is embedded in this linkage and to the relatively large M1−L bond length changes during the $^{HS}Co^{II} \rightarrow {}^{LS}Co^{III}$ transition in the central $[Co(\mu\text{-}NC)_6]$ moiety. The excess of Co over Fe precludes the bulk transition, which can be correlated with a significant decrease in the number of active electron transfer Fe-NC-W linkages, and the simultaneous increase in the number of $Co(O_3N_3)$-NC-W linkages, which favor spin transitions much less. This suggests a unique type of cooperativity over the whole series, which is unprecedented in the area of magnetochemistry. Interestingly, in the pure iron congener **0**, the oxidation of $^{HS}Fe^{II}$ to $^{HS}Fe^{III}$ itself does not result in large changes of M−L bond length compared to the transition from $^{HS}Co^{II}$ to $^{LS}Co^{III}$. However, we took into account some contribution of alternative $^{HS}Fe^{II} \rightarrow {}^{LS}Fe^{II}$ SCO process, occurring fractionally. This process assumes a huge local bond length changes and may coactivate the overall transition on the atomic scale.

A separate remark should be devoted to the matter of an inherently polydispersive character of phases **1**−**8**. The physical appearance, crystallographic features and physical properties of single crystals (SC XRD) or single crystal batches (PXRD, DSC and magnetic data) can reasonably label each family member in an unequivocal and repeatable manner, according to the used stoichiometric amounts of reagents. Moreover, the properties change systematically and continuously with the composition which indicates solid solution phases character of the series. Furthermore, we are able to prove the presence of $Co^{II}$ in the central position M1. On the other hand, we neither give the unequivocal information on the exact distribution of 3d ions in position M2−M5 in one cluster, nor do we ensure the identical composition of the clusters composing a single crystal of the selected phase. The latter means that e.g., the phase marked as **2**, $\{Fe_7Co_2W_6\}$ should be composed mainly of $\{Fe_7Co_2W_6\}$ clusters but accompanied by statistically distributed $\{Fe_6Co_3W_6\}$ and $\{Fe_8CoW_6\}$ clusters. Such polydispersion contribute to the characteristics of single crystals, but does not need to significantly modify bulk transitions properties.

The presented study showed the remarkable possibility to selectively induce the charge transfer properties or slow magnetic relaxation effects in one molecular framework of the $\{Fe_{9-x}Co_xW_6\}$ clusters through the control of the metal composition. Such a result strongly contributes to research efforts on switchable and functional molecular magnets, and open a few promising perspectives. Particular attention should be given, from now on, to the coexisting Co-NC-W and Fe-NC-W linkages, which turn out to be efficient molecular platforms for two simultaneous electron transfer effects. Furthermore, the chemical modifications can be done to target novel polymetallic combinations of $M^{II}$ and $M'^{V}$ sites within the $\{M^{II}{}_9M'^{V}{}_6\}$ clusters, novel coordination spheres on the external M2−M5 positions, and further expansion of coordination skeleton using functional ligands and complexes, including the recent findings on chiral or luminescent M-$[M'(CN)_8]$ systems.[5d,6c] All these routes should amend the magnetic functionalities, exploring also the multifunctional potential of these advanced molecular materials.

## EXPERIMENTAL SECTION

**Materials and Syntheses.** All chemicals and materials were provided by commercial sources (Sigma-Aldrich, Idalia), and used without further purification. The $K_4[W^{IV}(CN)_8]\cdot 2H_2O$ salt, and the subsequent $Na_3[W^{V}(CN)_8]\cdot 4H_2O$ and $TBA_3[W^{V}(CN)_8]$ (TBA = tetrabutylammonium cation) precursors were obtained according to the literature procedures.[42] The single crystals of **0**−**9** were synthesized by the modification of the procedure applied for the $\{Fe_9W_6\}$ and $\{Co_3Fe_6W_6\}$ analogues.[17,29] The methanolic solution (3 mL) of $Na_3[W^{V}(CN)_8]\cdot 4H_2O$ (107 mg, 0.2 mmol) was quickly mixed with the methanolic solution (6 mL) of 3d metal ions (Fe, Co) mixture in a test tube. The amounts of Fe and Co salts were adapted to keep the total number of moles equals 0.3 mmol, and the relevant Fe:Co molar ratio as expected in the final product: 8:1 (**1**), 7:2 (**2**) 6:3 (**3**), 5:4 (**4**), 4:5 (**5**) 3:6 (**6**), 2:7 (**7**), 1:8 (**8**). For pure $\{Fe_9W_6\}$ and $\{Co_9W_6\}$, only one type of 3d metal ion with the amount of 0.3 mmol was used. Detailed amount of precursors used in the syntheses are collected in Table S1a. The identical results of the syntheses were obtained while using the organic $TBA_3[W^{V}(CN)_8]$ precursor in the appropriate molar ratio.

The resulting mixtures were vigorously shaken, closed with parafilm, and left for crystallization in the dark. The precipitates of the hue color identical to the color of the relevant solution appeared immediately. After several days, the tubes contained a weakly colored solution, a precipitate on its bottom, and a large amount of block crystals of the relevant color on the walls. The crystals were identified as $\{Fe_{9-x}Co_x[W(CN)_8]_6(MeOH)_{24}\}\cdot 12MeOH$ ($x$ = 0−8; named **0**−**8**) by X-ray monocrystalline diffraction with the support of the Fe:Co:W composition deduced from SEM EDS analysis, which was found to be in a good agreement with the d metal ions stoichiometry of the mother solution (Table S2).

While washed with MeOH and exposed to the air, the crystals of **0**−**9** exchange quickly MeOH molecules to $H_2O$ molecules, to reach the stable compositions of $\{Fe_{9-x}Co_x[W(CN)_8]_6\}\cdot 32H_2O$ ($x$ = 0−9; named **0hyd**−**9hyd**) as was confirmed by (C, N, H) elemental analysis (Table S1b), and infrared spectra in KBr pellets, according to the protocols reported recently.[17,29,32]

**Physical Techniques.** CHN elemental analyses for the hydrated samples of **0hyd**−**9hyd** were performed on a EuroEA EuroVector elemental analyzer. Molar ratios of $d$ metal centers in **0hyd**−**9hyd** were determined using Hitachi S-4700 SEM microscope equipped with EDS NORAN Vantage microanalysis system. To prevent the decomposition of the investigated material, the most of physical measurements were performed on the crystals placed in the mother liquid (**0**−**9@MeOH**), or dispersed in Apiezon N grease (**0**−**9@ap**). Powder X-ray diffraction patterns for **No.@MeOH** sealed in glass capillary (0.5 mm) were collected on a PANalytical X'Pert PRO MPD diffractometer with Debye−Scherrer geometry using CuK$\alpha$ radiation ($\lambda$ = 1.54187 Å; 2$\theta$ range: 3−85° for RT). Temperature dependent measurements were performed using the same device with Oxford Cryostream add-on in two modes: cooling (280 K → 150 K) and heating (150 K → 293 K) with the proper temperature stabilization time for each measurement, and the 2$\theta$ range of 4−40°. Cell parameters for 293 K (**HT**) and 150 K (**LT**) were refined using Jana2006 Software[43a] on the basis of single crystal data as starting parameters (cell parameters and space group but not cell


DOI: 10.1021/jacs.5b11924
J. Am. Chem. Soc. 2016, 138, 1635−1646

contents). DSC signals for **No.@MeOH** in the 150−300 K range were measured on a Mettler Toledo DSC 822$^e$ calorimeter. Magnetic measurements were performed for **No.@MeOH** using a Quantum Design SQUID magnetometer for crystals covered by a pure methanol in a sealed glass tube. Samples were initially cooled in zero field to freeze MeOH and to avoid alignment of the grains along external field. The magnetic data were corrected for the estimated diamagnetism of the holder, solvent, and diamagnetic components. Variable temperature infrared spectra of **No.@ap** were recorded using an EXCALIBUR FTS-3000 spectrometer. During the experiments, the spectrometer was purged with dry nitrogen. The measurements were carried out during cooling and heating with 2−3 K interval. The samples were sandwiched between two KRS-5 window disks. The Mössbauer spectra of the selected $\{Fe_{9-x}Co_xW_6\}$ samples for $x = 0-4$, (**0−4@ap**) were recorded in the transmission geometry in the temperature range between 295 and 80 K using a Wissel spectrometer with a bath cryostat. The temperature stabilization was better than 0.1 K, with the exception of RT experiments when the temperature varied between 293 and 297 K. The temperature distribution over the sample was less than 1 K as determined from the independent experiment. The powdered samples were mixed with vacuum grease Apiezon N, distributed in cupper ring, 12 mm in diameter, and covered with Al foil. Because of the small resonant absorption effects, especially at room temperature, the spectra were collected within 1−3 days.

**Crystal Structure Determination.** X-ray diffraction analyses were performed on the selected single crystals of **0−8** both at high (250 K, $\mathbf{0-8}^{HT}$), and low (130 K, $\mathbf{0-8}^{LT}$) temperature (Tables S3−S6). The diffraction data of all samples were collected on a RIGAKU R-AXIS RAPID imaging plate area detector equipped with graphite monochromated Mo K$\alpha$ X-ray radiation. The temperature was controlled by a XR-CS10K cryostat system of the Japan Thermal Engineering. The single crystals were taken from the mother solution and covered by Apiezon N grease, mounted on Micro Mounts, and measured at 250(2) K as a high temperature phase, $\mathbf{0-8}^{HT}$. After finishing the measurement of $\mathbf{0-8}^{HT}$, the crystal was slowly cooled down to 130(2) with the rate of 1 K·min$^{-1}$. This was followed by the stabilization of temperature for ca. 1 h, and then the measurement of the low temperature phase, $\mathbf{0-8}^{LT}$, was conducted.

The crystal structure of all phases, $\mathbf{0-8}^{HT}$ and $\mathbf{0-8}^{LT}$, were solved by a direct method using SHELXS-97, and refined by a full-matrix least-squares technique using SHELXL-2014/7.[43b] Calculations were performed by using partially Crystal Structure software package, and partially WinGX (ver. 1.80.05) system. Structural diagrams were prepared using Mercury 3.5.1. For the precise comparison between low and high temperature phases, the identical coordinate sets were applied in the refinements of all structures. The crystal structure of $\mathbf{0}^{LT}$ was used as a starting point, and the obtained coordinate set was applied in the refinement of subsequent phases. As a result, all phases **0−9** were primarily refined with Fe centers occupying all the 3d metal positions. The assignment of Co or Fe, according to the metal ratio obtained from SEM EDS analysis, was performed after the anisotropic refinement of all intracluster non-hydrogen atoms. This assignment was based on the analysis on the changes in the M-N/O bond lengths on going from HT to LT phase, assuming that the larger changes of bond lengths should be ascribed to the $^{HS}Co^{II}W^{V} \rightarrow {}^{LS}Co^{III}W^{IV}$ CTIST process, and thus suggest the dominated presence of Co on the indicated metal sites. The metal sites showing smaller changes in bond lengths were ascribed to Fe as the $^{HS}Fe^{II} \rightarrow {}^{HS}Fe^{III}$ CT process induce much smaller shifts in bond lengths.[29] The results of the Co/Fe assignment and detailed structural parameters of $\mathbf{0-9}^{HT}$ and $\mathbf{0-9}^{LT}$ are collected in Tables S7−S8. Except of few disordered carbon atoms of coordinated methanol molecules described by partial occupancies, all non-hydrogen atoms of cluster cores were refined anisotropically, while non-hydrogen atoms of solvent molecules were refined isotropically. Hydrogen atoms attached to carbon atoms of coordinated methanol molecules were positioned with an idealized geometry, and refined using a riding model. Both in HT and LT phases, the structural disorder was detected for part of terminal cyanides, and for both methanol molecules. Thus, to ensure the proper geometry, and to control the convergence of the refinement, some C−O distances were restrained by DFIX commands, and some restraints for thermal ellipsoids (DFIX) for carbon atoms of terminal methanol and cyanide ligands were applied. In a few cases, the splittings of the cyanides and carbon atoms of methanol molecules into two alternative positions with partial occupancies were calculated. The hydrogen atoms of solvent molecules and hydroxyl groups of all methanol molecules were unreachable. All crystallographic data were deposited in the CCDC database with the deposition numbers 1435345−1435362

## ■ ASSOCIATED CONTENT

### Supporting Information

The Supporting Information is available free of charge on the ACS Publications website at DOI: 10.1021/jacs.5b11924.

Results of SEM EDS analyses. Structure refinement. Detailed analysis of structural data, including analysis of M−L distances during the phase transitions, and the discussion on the directional character of the phase transitions. Thermal hysteresis parameters from PXRD, DSC and magnetic measurements. Temperature dependent IR spectra for selected compounds. Temperature variable $^{57}$Fe Mössbauer spectra with the detailed discussion, and summary of Mössbauer parameters of **1−4**. Additional magnetic characteristics, including field dependences of magnetization at 1.8 K, and frequency dependent *ac* magnetic susceptibilities for all samples. (PDF)

Crystal data. (CIF)

Crystal data. (CIF)

## ■ AUTHOR INFORMATION


### Corresponding Authors

*ohkoshi@chem.s.u-tokyo.ac.jp

*podgajny@chemia.uj.edu.pl


### Notes

The authors declare no competing financial interest.

## ■ ACKNOWLEDGMENTS


This work was financed by the Polish National Science Centre within the SONATA BIS Project UMO-2014/14/B/ST5/00357. The research was carried out with the equipment purchased thanks to the financial support of the European Regional Development Fund in the framework of the Polish Innovation Economy Operational Program (Contract No. POIG.02.01.00-12-023/08). S. Chorazy is grateful for the financial support of the Foundation for Polish Science within a START fellowship (2015 Edition), and for the financial support of the Polish Ministry of Science and Higher Education within the Iuventus Plus Programme 2015-2017 (Grant No. IP2014 006073). S. Ohkoshi acknowledges the JSPS for the financial support within the Grant-in-Aid for Specially Promoted Research (Grant Number 15H05697), and the Core Research for Evolutional Science and Technology (CREST) program of the Japan Science and Technology Agency (JST). K. Nakabayashi is grateful for the support of Grant-in Aid for Challenging Exploratory Research (Grant No. 15K13666). M. Kozieł acknowledges the financial support of the Polish Ministry of Science and Higher Education within the Iuventus Plus Programme 2013-2016 (Grant No. IP2012 017772)


## ■ REFERENCES


(1) (a) Tanase, S.; Tuna, F.; Guionneau, P.; Maris, T.; Rombaut, G.; Mathoniére, C.; Andruh, M.; Kahn, O.; Sutter, J.-P. *Inorg. Chem.* **2003**, *42*, 1625−1631. (b) Pinkowicz, D.; Podgajny, R.; Gaweł, B.; Nitek, W.;




DOI: 10.1021/jacs.5b11924
*J. Am. Chem. Soc.* 2016, 138, 1635−1646

Łasocha, W.; Makarewicz, M.; Bałanda, M.; Sieklucka, B. *Angew. Chem., Int. Ed.* **2011**, *50*, 3973−3977. (c) Wang, Q.-L.; Southerland, H.; Li, J.-R.; Prosvirin, A. V.; Zhao, H.; Dunbar, K. R. *Angew. Chem., Int. Ed.* **2012**, *15*, 9321−9324. (d) Nowicka, B.; Reczyński, M.; Rams, M.; Nitek, W.; Kozieł, M.; Sieklucka, B. *CrystEngComm* **2015**, *17*, 3526−2532.

(2) (a) Maspoch, D.; Ruiz-Molina, D.; Wurst, K.; Domingo, N.; Cavallini, M.; Biscarini, F.; Tejada, J.; Rovira, C.; Veciana, J. *Nat. Mater.* **2003**, *2*, 190−195. (b) Dechambenoit, P.; Long, J. R. *Chem. Soc. Rev.* **2011**, *40*, 3249−3265. (c) Coronado, E.; Gimenez-Marques, M.; Espallargas, G. M.; Brammer, L. *Nat. Commun.* **2012**, *3*, 828. (d) Coronado, E.; Espallargas, G. M. *Chem. Soc. Rev.* **2013**, *42*, 1525−1539.

(3) (a) Sato, O.; Iyoda, T.; Fujishima, A.; Hashimoto, K. *Science* **1996**, *272*, 704−705. (b) Shimamoto, N.; Ohkoshi, S.; Sato, O.; Hashimoto, K. *Inorg. Chem.* **2002**, *41*, 678−684. (c) Tokoro, H.; Ohkoshi, S.; Matsuda, T.; Hashimoto, K. *Inorg. Chem.* **2004**, *43*, 5231−5236. (d) Avendano, C.; Hilfiger, M. G.; Prosvirin, A.; Sanders, C.; Stepien, D.; Dunbar, K. R. *J. Am. Chem. Soc.* **2010**, *132*, 13123−13125.

(4) (a) Coronado, E.; Galan-Mascaros, J. R.; Gomez-Garcia, C. J.; Laukhin, V. *Nature* **2000**, *408*, 447−449. (b) Galan-Mascaros, J. R.; Coronado, E.; Goddard, P. A.; Singleton, J.; Coldea, A. I.; Wallis, J. D.; Coles, S. J.; Alberola, A. *J. Am. Chem. Soc.* **2010**, *132*, 9271−9273. (c) Ohkoshi, S.; Nakagawa, K.; Tomono, K.; Imoto, K.; Tsunobuchi, Y.; Tokoro, H. *J. Am. Chem. Soc.* **2010**, *132*, 6620−6621. (d) Pardo, E.; Train, C.; Gontard, G.; Boubekeur, K.; Fabelo, O.; Liu, H.; Dkhil, B.; Lloret, F.; Nakagawa, K.; Tokoro, H.; Ohkoshi, S.; Verdaguer, M. *J. Am. Chem. Soc.* **2011**, *133*, 15328−15331.

(5) (a) Ma, L.; Abney, C.; Lin, W. *Chem. Soc. Rev.* **2009**, *38*, 1248−1256. (b) Train, C.; Gruselle, M.; Verdaguer, M. *Chem. Soc. Rev.* **2011**, *40*, 3297−3312. (c) Wanderley, M. M.; Wang, C.; Wu, C.-D.; Lin, W. *J. Am. Chem. Soc.* **2012**, *134*, 9050−9053. (d) Chorazy, S.; Nakabayashi, K.; Imoto, K.; Mlynarski, J.; Sieklucka, B.; Ohkoshi, S. *J. Am. Chem. Soc.* **2012**, *134*, 16151−16154.

(6) (a) Cui, Y.; Yue, Y.; Qian, G.; Chen, B. *Chem. Rev.* **2012**, *112*, 1126−1162. (b) Chelebaeva, E.; Larionova, J.; Guari, Y.; Ferreira, R. A. S.; Carlos, L. D.; Almeida Paz, F. A.; Trifonov, A.; Guerin, C. *Inorg. Chem.* **2009**, *48*, 5983−5995. (c) Chorazy, S.; Nakabayashi, K.; Ohkoshi, S.; Sieklucka, B. *Chem. Mater.* **2014**, *26*, 4072−4075. (d) Feng, M.; Pointillart, M.; Lefeuvre, B.; Dorcet, V.; Golhen, S.; Cador, O.; Ouahab, L. *Inorg. Chem.* **2015**, *54*, 4021−4028.

(7) (a) Mohopatra, S.; Rajeswaran, B.; Chakraborty, A.; Sundaresan, A.; Kumar Maji, T. *Chem. Mater.* **2013**, *25*, 1673−1679. (b) Guo, P.-H.; Meng, Y.; Chen, Y.-C.; Li, Q.-W.; Wang, B.-Y.; Leng, J.-D.; Bao, D.-H.; Jia, J.-H.; Tong, M.-L. *J. Mater. Chem. C* **2014**, *2*, 8858−8864. (c) Abherve, A.; Manas-Valero, S.; Clemente-Leon, M.; Coronado, E. *Chem. Sci.* **2015**, *6*, 4665−4673. (d) Long, J.; Rouquette, J.; Thibaud, J.-M.; Ferreira, R. A. S.; Carlos, L. D.; Donnadieu, B.; Vieru, V.; Chibotaru, L. F.; Konczewicz, L.; Haines, J.; Guari, Y.; Larionova, J. *Angew. Chem., Int. Ed.* **2015**, *54*, 2236−2240.

(8) (a) Ohkoshi, S.; Imoto, K.; Tsunobuchi, Y.; Takano, S.; Tokoro, H. *Nat. Chem.* **2011**, *3*, 564−569. (b) Ohkoshi, S.; Tokoro, H. *Acc. Chem. Res.* **2012**, *45*, 1749−1758. (c) Matsumoto, T.; Newton, G. N.; Shiga, T.; Hayami, S.; Matsui, Y.; Okamoto, H.; Kumai, R.; Murakami, Y.; Oshio, H. *Nat. Commun.* **2014**, *5*, 3865. (d) Koumousi, E. S.; Jeon, I.-R.; Gao, Q.; Dechambenoit, P.; Woodruff, D. N.; Merzeau, P.; Buisson, L.; Jia, X.; Li, D.; Volatron, F.; Mathoniere, C.; Clerac, R. *J. Am. Chem. Soc.* **2014**, *136*, 15461−15464. (e) Arai, M.; Kosaka, W.; Matsuda, T.; Ohkoshi, S. *Angew. Chem., Int. Ed.* **2008**, *47*, 6885−6887.

(9) (a) Pardo, E.; Train, C.; Liu, H.; Chamoreau, L. M.; Dhkil, B.; Boubekeur, K.; Lloret, F.; Nakatani, K.; Tokoro, H.; Ohkoshi, S.; Verdaguer, M. *Angew. Chem., Int. Ed.* **2012**, *51*, 8356−8360. (b) Canadillas-Delgado, L.; Fabelo, O.; Rodriguez-Velamazan, J. A.; Lemee-Cailleau, M.-H.; Mason, S. A.; Pardo, E.; Lloret, F.; Zhao, J.-P.; Bu, X.-H.; Simonet, V.; Colin, C. V.; Rodriguez-Carvajal, J. *J. Am. Chem. Soc.* **2012**, *134*, 19772−19781. (c) Castellano, M.; Ruiz-García, R.; Cano, J.; Ferrando-Soria, J.; Pardo, E.; Fortea-Perez, F. R.; Stiriba, S.-E.; Julve, M.; Lloret, F. *Acc. Chem. Res.* **2015**, *48*, 510−520.

(10) (a) Train, C.; Gheorghe, R.; Krstic, V.; Chamoreau, L.-M.; Ovanesyan, N. S.; Rikken, G. L. J. A.; Gruselle, M.; Verdaguer, M. *Nat. Mater.* **2008**, *7*, 729−734. (b) Pinkowicz, D.; Podgajny, R.; Nitek, W.; Rams, M.; Majcher, A. M.; Nuida, T.; Ohkoshi, S.; Sieklucka, B. *Chem. Mater.* **2011**, *23*, 21−31. (c) Ohkoshi, S.; Takano, S.; Imoto, K.; Yoshikiyo, M.; Namai, A.; Tokoro, H. *Nat. Photonics* **2014**, *8*, 65−71.

(11) Shiga, T.; Tetsuka, T.; Sakai, K.; Sekine, Y.; Nihei, M.; Newton, G. N.; Oshio, H. *Inorg. Chem.* **2014**, *53*, 5899−5901.

(12) (a) Li, D.; Clérac, R.; Roubeau, O.; Harté, E.; Mathonière, C.; Le Bris, R.; Holmes, S. M. J. *J. Am. Chem. Soc.* **2008**, *130*, 252−258. (b) Siretanu, D.; Li, D.; Buisson, L.; Bassani, D. M.; Holmes, S. M.; Mathonière, C.; Clérac, R. *Chem. - Eur. J.* **2011**, *17*, 11704−11708. (c) Mitsumoto, K.; Oshiro, E.; Nishikawa, H.; Shiga, T.; Yamamura, Y.; Saito, K.; Oshio, H. *Chem. - Eur. J.* **2011**, *17*, 9612−9618. (d) Nihei, M.; Sekine, Y.; Suganami, N.; Nakazawa, K.; Nakao, A.; Nakao, H.; Murakami, Y.; Oshio, H. *J. Am. Chem. Soc.* **2011**, *133*, 3592−3600. (e) Nihei, M.; Okamoto, Y.; Sekine, Y.; Hoshino, N.; Shiga, T.; Liu, I. P.-C.; Oshio, H. *Angew. Chem., Int. Ed.* **2012**, *51*, 6361−6364. (f) Dong, D.-P.; Liu, T.; Kanegawa, S.; Kang, S.; Sato, O.; He, C.; Duan, C.-Y. *Angew. Chem., Int. Ed.* **2012**, *51*, 5119−5123. (g) Liu, T.; Dong, D.-P.; Kanegawa, S.; Kang, S.; Sato, O.; Shiota, Y.; Yoshizawa, K.; Hayami, S.; Wu, S.; He, C.; Duan, C.-Y. *Angew. Chem., Int. Ed.* **2012**, *51*, 4367−4370.

(13) (a) Ohkoshi, S.; Hamada, Y.; Matsuda, T.; Tsunobuchi, Y.; Tokoro, H. *Chem. Mater.* **2008**, *20*, 3048−3054. (b) Ozaki, N.; Tokoro, H.; Hamada, Y.; Namai, A.; Matsuda, T.; Kaneko, S.; Ohkoshi, S. *Adv. Funct. Mater.* **2012**, *22*, 2089−2093. (c) Mondal, A.; Chamoreau, L.-M.; Li, Y.; Journaux, Y.; Seuleiman, M.; Lescouëzec, R. *Chem. - Eur. J.* **2013**, *19*, 7682−7685. (d) Ozaki, N.; Tokoro, H.; Miyamoto, Y.; Ohkoshi, S. *New J. Chem.* **2014**, *38*, 1950−1954.

(14) Liu, T.; Zheng, H.; Kang, S.; Shiota, Y.; Hayami, S.; Mito, M.; Sato, O.; Yoshizawa, K.; Kanegawa, S.; Duan, C. *Nat. Commun.* **2013**, *4*, 2826.

(15) Pinkowicz, D.; Rams, M.; Mišek, M.; Kamenev, K. V.; Tomkowiak, H.; Katrusiak, A.; Sieklucka, B. *J. Am. Chem. Soc.* **2015**, *137*, 8795−8802.

(16) Hilfiger, M. G.; Chen, M.; Brinzari, T. V.; Nocera, T. M.; Shatruk, M.; Petasis, D. T.; Musfeldt, J. L.; Achim, C.; Dunbar, K. R. *Angew. Chem., Int. Ed.* **2010**, *49*, 1410−1413.

(17) Chorazy, S.; Podgajny, R.; Nogaś, W.; Nitek, W.; Kozieł, M.; Rams, M.; Juszyńska-Gałązka, E.; Żukrowski, J.; Kapusta, C.; Nakabayashi, K.; Fujimoto, T.; Ohkoshi, S.; Sieklucka, B. *Chem. Commun.* **2014**, *49*, 3484−3487.

(18) Nowicka, B.; Reczyński, M.; Rams, M.; Nitek, W.; Żukrowski, J.; Kapusta, C.; Sieklucka, B. *Chem. Commun.* **2015**, *51*, 11485−11488.

(19) (a) Gatteschi, D.; Sessoli, R. *Angew. Chem., Int. Ed.* **2003**, *42*, 268−297. (b) Murrie, M. *Chem. Soc. Rev.* **2010**, *39*, 1986−1995.

(20) (a) Tomsa, A.-R.; Martínez-Lillo, J.; Li, Y.; Chamoreau, L.-M.; Boubekeur, K.; Farias, F.; Novak, M. A.; Cremades, E.; Ruiz, E.; Proust, A.; Verdaguer, M.; Gouzerh, P. *Chem. Commun.* **2010**, *46*, 5106−5108. (b) Suna, H.-L.; Wang, Z.-M.; Gao, S. *Coord. Chem. Rev.* **2010**, *254*, 1081−1100. (c) Gomez-Coca, S.; Cremades, E.; Aliaga-Alcalde, N.; Ruiz, E. *J. Am. Chem. Soc.* **2013**, *135*, 7010−7018. (d) Zazdrozny, J. M.; Xiao, D. J.; Atanasov, M.; Long, G. J.; Grandjean, F.; Neese, F.; Long, J. R. *Nat. Chem.* **2013**, *5*, 577−581. (e) Herchel, R.; Váhovská, L.; Potočňák, I.; Trávníček, Z. *Inorg. Chem.* **2014**, *53*, 5896−5898.

(21) (a) Sessoli, R.; Powell, A. K. *Coord. Chem. Rev.* **2009**, *253*, 2328−2341. (b) Woodruff, D. N.; Winpenny, R. E. P.; Layfield, R. A. *Chem. Rev.* **2013**, *113*, 5110−5148. (c) Blagg, R. J.; Ungur, L.; Tuna, F.; Speak, J.; Comar, P.; Collison, D.; Wernsdorfer, W.; McInnes, E. J.; Chibotaru, L. F.; Winpenny, R. E. P. *Nat. Chem.* **2013**, *5*, 673−678. (d) Brown, A. J.; Pinkowicz, D.; Saber, M.; Dunbar, K. R. *Angew. Chem., Int. Ed.* **2015**, *54*, 5864−5868.

(22) (a) Mishra, A.; Wernsdorfer, W.; Parsons, S.; Christou, G.; Brechin, E. *Chem. Commun.* **2005**, 2086−2088. (b) Hołyńska, M.; Premužić, D.; Jeon, I.-R.; Wernsdorfer, W.; Clérac, R.; Dehnen, S. *Chem. - Eur. J.* **2011**, *17*, 9605−9610. (c) Liu, K.; Shi, W.; Cheng, P. *Coord. Chem. Rev.* **2015**, *289*−*290*, 74−122. (d) Langley, S. K.; Le, C.; Ungur, L.; Moubaraki, B.; Abrahams, B. F.; Chibotaru, L. F.; Murray, K. S. *Inorg. Chem.* **2015**, *54*, 3631−3642.

(23) (a) Li, D.; Clérac, R.; Parkin, S.; Wang, G.; Yee, G. T.; Holmes, S. M. *Inorg. Chem.* **2006**, *45*, 5251−5253. (b) Visinescu, D.; Madalan, A.



DOI: 10.1021/jacs.5b11924
*J. Am. Chem. Soc.* 2016, 138, 1635−1646

M.; Andruh, M.; Duhayon, C.; Sutter, J.-P.; Ungur, L.; Van den Heuvel, W.; Chibotaru, L. F. *Chem. - Eur. J.* **2009**, *15*, 11808−11814. (c) Venkatakrishnan, T. S.; Sahoo, S.; Bréfuel, N.; Duhayon, C.; Paulsen, C.; Barra, A.-L.; Ramasesha, S.; Sutter, J.-P. *J. Am. Chem. Soc.* **2010**, *132*, 6047−6056. (d) Zadrozny, J. M.; Freedman, D. E.; Jenkins, D. M.; Harris, T. D.; Iavarone, A. T.; Mathonière, C.; Clérac, R.; Long, J. R. *Inorg. Chem.* **2010**, *49*, 8886−8896. (e) Zhang, Y.-Z.; Mallik, U. P.; Clérac, R.; Rath, N. P.; Holmes, S. M. *Chem. Commun.* **2011**, *47*, 7194−7196. (f) Zhang, Y.-Z.; Mallik, U. P.; Clérac, R.; Rath, N. P.; Holmes, S. M. *Chem. Commun.* **2011**, *47*, 7194−7196.

(24) (a) Bogani, L.; Wernsdorfer, W. *Nat. Mater.* **2008**, *7*, 179−186. (b) Mannini, M.; Pineider, F.; Sainctavit, P.; Danieli, C.; Otero, E.; Sciancalepore, C.; Talarico, A. M.; Arrio, M.-A.; Cornia, A.; Gatteschi, D.; Sessoli, R. *Nat. Mater.* **2009**, *8*, 194−197. (c) Urdampilleta, M.; Klayatskaya, S.; Ruben, M.; Wernsdorfer, W. *ACS Nano* **2015**, *9*, 4458−4464.

(25) (a) Shatruk, M.; Avendano, C.; Dunbar, K. R. In *Prog. Inorg. Chem.*; Karlin, K. D., Ed.; John Wiley & Sons: Hoboken, NJ, 2009; Vol. *56*, pp 155−334. (b) Pinkowicz, D.; Podgajny, R.; Nowicka, B.; Chorazy, S.; Reczyński, M.; Sieklucka, B. *Inorg. Chem. Front.* **2015**, *2*, 10−27.

(26) (a) Li, D.; Parkin, S.; Wang, G.; Yee, G. T.; Clérac, R.; Wernsdorfer, W.; Holmes, S. M. *J. Am. Chem. Soc.* **2006**, *128*, 4214−4215. (b) Shiga, T.; Newton, G. N.; Mathieson, J. S.; Tetsuka, T.; Nihei, M.; Cronin, L.; Oshio, H. *Dalton Trans.* **2010**, *39*, 4730−4733. (c) Wang, X.-Y.; Prosvirin, A. V.; Dunbar, K. R. *Angew. Chem., Int. Ed.* **2010**, *49*, 5081−5084. (d) Nowicka, B.; Näther, C.; Halemba, A.; Reczyński, M.; Sieklucka, B. *Dalton Trans.* **2015**, *44*, 1780−12787.

(27) Kang, S.; Zheng, H.; Liu, T.; Hamachi, K.; Kanegawa, S.; Sugimoto, K.; Shiota, Y.; Hayami, S.; Mito, M.; Nakamura, T.; Nakano, M.; Baker, M. L.; Nojiri, H.; Yoshizawa, K.; Duan, C.; Sato, O. *Nat. Commun.* **2014**, *6*, 5955.

(28) (a) Zhong, Z. J.; Seino, H.; Mizobe, Y.; Hidai, M.; Fujishima, A.; Ohkoshi, S.; Hashimoto, K. *J. Am. Chem. Soc.* **2000**, *122*, 2952−2953. (b) Song, Y.; Zhang, P.; Ren, X.-M.; Shen, X.-F.; Li, Y.-Z.; You, X.-Z. *J. Am. Chem. Soc.* **2005**, *127*, 3708−3709. (c) Bonadio, F.; Gross, M.; Stoeckli-Evans, H.; Decurtins, S. *Inorg. Chem.* **2002**, *41*, 5891−5896.

(29) Podgajny, R.; Chorazy, S.; Nitek, W.; Rams, M.; Majcher, A. M.; Marszałek, B.; Żukrowski, J.; Kapusta, C.; Sieklucka, B. *Angew. Chem., Int. Ed.* **2013**, *52*, 896−900.

(30) Freedman, D. E.; Bennett, M. V.; Long, J. R. *Dalton Trans.* **2006**, 2829−2834.

(31) Hilfiger, M. G.; Zhao, H.; Prosvirin, A. V.; Wernsdorfer, W.; Dunbar, K. R. *Dalton Trans.* **2009**, 5155−5163.

(32) (a) Chorazy, S.; Podgajny, R.; Nitek, W.; Rams, M.; Ohkoshi, S.; Sieklucka, B. *Cryst. Growth Des.* **2013**, *13*, 3036−3045. (b) Chorazy, S.; Reczyński, M.; Podgajny, R.; Nogaś, W.; Buda, S.; Rams, M.; Nitek, W.; Nowicka, B.; Mlynarski, J.; Ohkoshi, S.; Sieklucka, B. *Cryst. Growth Des.* **2015**, *15*, 3573−3581.

(33) Chorazy, S.; Podgajny, R.; Nakabayashi, K.; Stanek, J.; Rams, M.; Sieklucka, B.; Ohkoshi, S. *Angew. Chem., Int. Ed.* **2015**, *54*, 5093−5097.

(34) (a) Ohkoshi, S.; Iyoda, T.; Fujishima, A.; Hashimoto, K. *Phys. Rev. B: Condens. Matter Mater. Phys.* **1997**, *56*, 11642−11652. (b) Hozumi, T.; Hashimoto, K.; Ohkoshi, S. *Phys. Rev. B: Condens. Matter Mater. Phys.* **2006**, *73*, 092409.

(35) (a) Wang, Y.-Q.; Cheng, A.-L.; Liu, P.-P.; Gao, E.-Q. *Chem. Commun.* **2013**, *49*, 6995−6997. (b) Wang, Y.-Q.; Yue, Q.; Qi, Y.; Wang, K.; Sun, Q.; Gao, E.-Q. *Inorg. Chem.* **2013**, *52*, 4259−4268. (c) Ruamps, R.; Batchelor, L. J.; Guillot, R.; Zakhia, G.; Barra, A.-L.; Wernsdorfer, W.; Guihery, N.; Mallah, T. *Chem. Sci.* **2014**, *5*, 3418−3424.

(36) (a) Hauser, A.; Jeftić, J.; Romstedt, H.; Hinek, R.; Spiering, H. *Coord. Chem. Rev.* **1999**, *190−192*, 471−491. (b) Zheng, S.; Siegler, M. A.; Costa, J. S.; Fu, W.-T.; Bonnet, S. *Eur. J. Inorg. Chem.* **2013**, *2013*, 1033−1042. (c) Lefter, C.; Tricard, S.; Peng, H.; Molnar, G.; Salmon, L.; Demont, P.; Rotaru, A.; Bousseksou, A. *J. Phys. Chem. C* **2015**, *119*, 8522−8529.

(37) (a) Cui, Y.; Xu, H.; Yue, Y.; Guo, Z.; Yu, J.; Chen, Z.; Gao, J.; Yang, Y.; Qian, G.; Chen, B. *J. Am. Chem. Soc.* **2012**, *134*, 3979−3982. (b) Chelebaeva, E.; Long, J.; Larionova, J.; Ferreira, R. A. S.; Carlos, L. D.; Almeida Paz, F. A.; Gomes, J. B. R.; Trifonov, A.; Guérin, C.; Guari, Y. *Inorg. Chem.* **2012**, *51*, 9005−9016. (c) Rao, X.; Song, T.; Gao, J.; Cui, Y.; Yang, Y.; Wu, C.; Chen, B.; Qian, G. *J. Am. Chem. Soc.* **2013**, *135*, 15559−15564.

(38) (a) Coey, J. M. D.; Viret, M.; von Molnar, S. *Adv. Phys.* **1999**, *48*, 167−293. (b) Yu, Z.; Zhang, N.; Yao, Z.; Han, X.; Jiang, Z. *J. Mater. Chem. A* **2013**, *1*, 12462−12470. (c) Wu, J.; Xiao, D.; Zhu, J. *Chem. Rev.* **2015**, *115*, 2559−2595.

(39) Przychodzeń, P.; Korzeniak, T.; Podgajny, R.; Sieklucka, B. *Coord. Chem. Rev.* **2006**, *250*, 2234−2260.

(40) (a) Pinkowicz, D.; Podgajny, R.; Pełka, R.; Nitek, W.; Bałanda, M.; Makarewicz, M.; Czapla, M.; Żukrowski, J.; Kapusta, C.; Zając, D.; Sieklucka, B. *Dalton Trans.* **2009**, 7771−7777. (b) Venkatakrishnan, T. S.; Duhayon, C.; Gogoi, N.; Sutter, J.-P. *Inorg. Chim. Acta* **2011**, *372*, 403−406. (c) Lloret, F.; Julve, M.; Cano, J.; Ruiz-Garcia, R.; Pardo, E. *Inorg. Chim. Acta* **2008**, *361*, 3432−3445.

(41) (a) Clima, S.; Hendrickx, M. F. A.; Chibotaru, L. F.; Soncini, A.; Mironov, V.; Ceulemans, A. *Inorg. Chem.* **2007**, *46*, 2682−2690. (b) Chorazy, S.; Podgajny, R.; Nogaś, W.; Buda, S.; Nitek, W.; Mlynarski, J.; Rams, M.; Kozieł, M.; Juszyńska Gałązka, E.; Vieru, V.; Chibotaru, L. F.; Sieklucka, B. *Inorg. Chem.* **2015**, *54*, 5784−5794.

(42) (a) Matoga, D.; Szklarzewicz, J.; Mikuriya, M. *Inorg. Chem.* **2006**, *45*, 7100−7104. (b) Samotus, A. *Polym. J. Chem.* **1973**, *47*, 653−657. (c) Pribush, R.; Archer, R. D. *Inorg. Chem.* **1974**, *13*, 2556−2563.

(43) (a) Petricek, V.; Dusek, M.; Palatinus, L. *Z. Kristallogr. - Cryst. Mater.* **2014**, *229*, 345−352. (b) Sheldrick, G. M. *Acta Crystallogr., Sect. A: Found. Crystallogr.* **2008**, *A64*, 112−122.



DOI: 10.1021/jacs.5b11924
*J. Am. Chem. Soc.* 2016, 138, 1635−1646